AWARD NUMBER: W81XWH-13-1-0409

TITLE: The Role of Skp2 in the Prostate Tumorigenesis Following Rb and p53 Loss

PRINCIPAL INVESTIGATOR: Hongling Zhao

CONTRACTING ORGANIZATION: Albert Einstein College of Medicine
Bronx, NY 10461

REPORT DATE: October 2014

TYPE OF REPORT: Annual Report

PREPARED FOR: U.S. Army Medical Research and Materiel Command
Fort Detrick, Maryland 21702-5012

REPORT DOCUMENTATION PAGE

Form Approved
OMB No. 0704-0188

1. REPORT DATE	2. REPORT TYPE	3. DATES COVERED
October 2014	Annual Report	26 Sep 2013 - 25 Sep 2014

4. TITLE AND SUBTITLE
The Role of Skp2 in the Prostate Tumorigenesis Following Rb and p53 Loss

5a. CONTRACT NUMBER

5b. GRANT NUMBER
W81XWH-13-1-0409

5c. PROGRAM ELEMENT NUMBER

6. AUTHOR(S)

Hongling Zhao

E-Mail:Hongling.zhao@einstein.yu.edu

5d. PROJECT NUMBER

5e. TASK NUMBER

5f. WORK UNIT NUMBER

7. PERFORMING ORGANIZATION NAME(S) AND ADDRESS(ES)

Albert Einstein College of Medicine of Yeshiva University
Department of Developmental and
Molecular Biology
Room 521 Ullmann
1300 Morris Park Avenue
Bronx, NY 10461-1975

8. PERFORMING ORGANIZATION REPORT NUMBER

9. SPONSORING / MONITORING AGENCY NAME(S) AND ADDRESS(ES)

U.S. Army Medical Research and Materiel Command
Fort Detrick, Maryland 21702-5012

10. SPONSOR/MONITOR'S ACRONYM(S)

11. SPONSOR/MONITOR'S REPORT NUMBER(S)

12. DISTRIBUTION / AVAILABILITY STATEMENT

Approved for Public Release; Distribution Unlimited

13. SUPPLEMENTARY NOTES

14. ABSTRACT

Genetic inactivation of both major tumor suppressors pRb and p53 irreparably disables most cells' antitumor mechanisms. TCGA documents recurrent genetic inactivation of RB1 and TP53. They often co-occur and the co-occurrences become more frequent in more advanced cancer, which likely explain why advanced cancer are more likely to resist current anticancer therapies. Here, we found that p53 activates expression of Pirh2 and KPC1, two of the three ubiquitin ligases for p27. Loss of p53 in the absence of Skp2, the third ubiquitin ligase for p27, shrinks the cellular pool of p27 ubiquitin ligases to accumulate p27 protein. In the absence of pRb and p53, p27 was unable to inhibit DNA synthesis in spite of its abundance, but could inhibit division of cells that maintain DNA replication with rereplication. This mechanism blocked pRb/p53 doubly deficient pituitary and prostate tumorigenesis lastingly coexistent with bromodeoxyuridine-labeling neoplastic lesions, revealing an unconventional cancer cell vulnerability when pRb and p53 are inactivated.

15. SUBJECT TERMS
pRb, p53, p27, Skp2, ubiquitin ligase, prostate cancer, tumorigenesis, safeguard

16. SECURITY CLASSIFICATION OF:			17. LIMITATION OF ABSTRACT	18. NUMBER OF PAGES	19a. NAME OF RESPONSIBLE PERSON
a. REPORT	b. ABSTRACT	c. THIS PAGE			19b. TELEPHONE NUMBER *(include area code)*
Unclassified	Unclassified	Unclassified	Unclassified	42	USAMRMC

Table of Contents

Page

INTRODUCTION:

pRb and p53 are the two of the best known tumor suppressor proteins. They play key roles in providing most and best of the cells' intrinsic antitumor mechanisms, such as proliferation arrest, cellular senescence, and apoptosis. pRb and p53 are frequently inactivated in cancer[1,2,3,4,5,6,7,8]. Reactivating pRb and p53 is a major goal of anticancer strategies. When pRb and p53 are genetically inactivated, cells would permanently lose the antitumor mechanisms provided by them. The Cancer Genome Atlas projects have shown that genetic inactivation of RB1 and TP53 is very common. Moreover, these mutations often cooccur, and the co-occurrences become more frequent in more advanced cancer, which likely explains why advanced cancer are more likely to resist current anticancer therapies. Finding successful treatments for more advanced and multi-therapy resistant cancers will likely depend on our ability to discover antitumor mechanisms that are effective when pRb and p53 are genetically inactivated. The purpose of this research is to determine whether deletion of Skp2 can block tumorigenesis following loss of pRb and p53 in mouse prostate tumor model[5]. The scope of the research is from the determine the role of Skp2 in prostate tumorigenesis induced by loss of both pRb and p53 to the dissection of the detail molecular mechanisms of the roles of Skp2 in the tumorigenesis by investigating whether the effects of Skp2 loss on prostate tumorigenesis is p27-dependent. Finally, we will determine the role of Skp2 in prostate stem cell and prostate cancer stem cell compartments since the prostate tumors from pRb and p53 double deficient mice is believed to arise from prostate stem cells[9].

KEYWORDS:

pRb, p53, ,Skp2, p27, Tumor Suppressors, Ubiquitin Ligase, Tumorigenesis, Stem Cells, Cancer Stem cells, Safeguard, Antitumor Mechanism

OVERALL PROJECT SUMMARY:

Task 1. To determine the roles of Skp2 in prostate tumorigenesis induced by loss of both pRb and p53 (Timeline 1-3 months).

I have finished Task 1. Please see attached paper in appendices for detail "Cancer Cell

2013 Nov 11;24(5):645-59".

Task 2. To determine whether Skp2's repressive effects on the prostate tumorigenesis is p27-dependent (Timeline: months 1-24).

Task 2a. p27T187A/T187A knock-in mice are available in our lab. We have set up breeding colonies in order to generate DKO;p27T187A/T187A (AADKO) male mice.

I already generated enough AADKO male mice and analyzed the phenotypes of these mice.

First, I made a survival curve and compared the survivals and pathological diagnoses of AADKO male mice with those of DKO male mice, which are shown in Figure 1A and 1B. p27T187A/T187A knockin significantly delay the death of DKO mice. The median survival of DKO mice is 8.47 month, while is 10.00 month for AADKO mice. Even though, it prolonged the survival of DKO mice, p27T187A/T187A knockin cannot completely phenocopy the effects of Skp2 deletion in DKO mice. Furthermore, p27T187A/T187A knockin delayed the progression of tumor by keeping the tumors at relatively low grades.

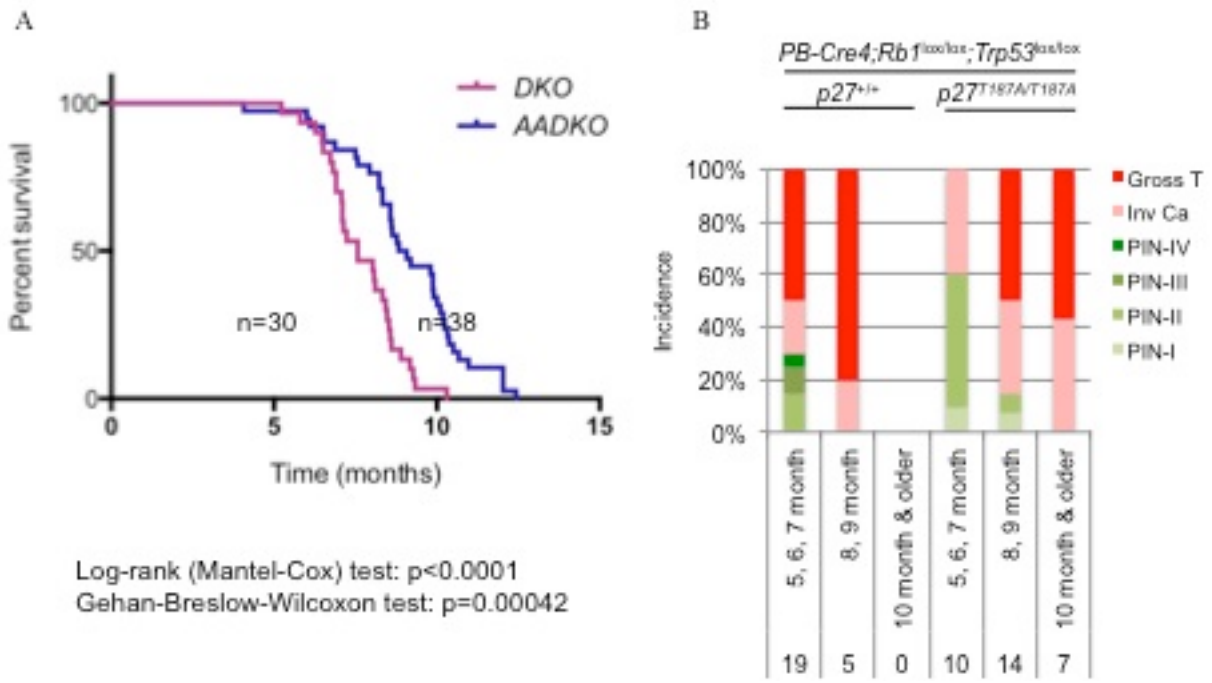

Figure 1 (A) Kaplan-Meier survival analysis of two cohorts of mice with indicated genotypes. (B) Pathological diagnoses of prostate lesions in mice of indicated genotypes in three age groups. Each prostate was serially sectioned and the most advanced lesions were the diagnoses. PIN, prostatic intraepithelial neoplasia.

I continued to characterize the phenotypes of tumors from AADKO mice by performing

HE staining and p27 staining. Figure 2 show that AADKO mice also contains higher levels of p27, as measured by immunohistochemistry analysis. I am going to further characterize the proliferation and apoptosis marker in AADKO mice, and compare the results with those from DKO and TKO mice.

Task 2b. To determine whether p27 is necessary for prostate tumorigenesis in this DKO model (Timeline: 1-24 months). We will generate at least 5 TKO;p27-/- male mice and littermate control.

Even though p27T187A/T187A knockin delays tumor progression and prolongs the survival of DKO mice, it cannot completely phenocopy the effect of Skp2 deletion in blocking prostate tumorigenesis in DKO mice, which indicates that the other functions of Skp2 might also contribute to the blockage of tumorigenesis. So next, I decided to further investigate what functions of Skp2 might play roles in our prostate tumor mouse model instead do further crossing to get TKO;p27-/- male mice.

In order to further dissect the other mechanism involved in Skp2's effect in tumorigenesis, I need to compare the different between DKO, TKO and AADKO prostates. I generated prostate cancer cell lines from the tumor masses of DKO and AADKO mice, and used these DKO and AADKO mouse prostate cell lines to further investigate other functions of Skp2. In order to mimic the TKO prostate, I knocked down Skp2 in those cells and determined the p27 levels and growth rates of the cells lines. Figure 3 shows that p27 level is dramatically increased after knocking down of Skp2 in DKO cell lines, while is not significantly changed in AADKO cell lines. Consistent with the IHC staining, p27 levels is much higher in AADKO cell lines compared to DKO cell lines, which might be the explanation for slow progression of tumor grades and prolonged survival of AADKO mice. Expectedly, Skp2 knockdown and p27T187A/T187A knockin slow down the growth rate of DKO cell lines, Interestingly, Skp2 knockdown further inhibit the proliferation of AADKO cell lines, which might caused by the other function of Skp2.

In addition to mediating ubiquitination of p27 to activate cyclin/CDKs, Skp2 can also ubiquitinate Akt1 to promote anaerobic glycolysis[10], and E-cadherin to promote cell migration[11]. Based on this platform, we are going to identify multiple antitumor mechanisms of Skp2, including apoptosis by p73, blocking anaerobic glycolysis by targeting LDH-A, and dynamic

control of EMT. We believe that we will identify multiple antitumor mechanisms of Skp2 in our pRb and p53 double deficient mouse prostate tumor model, which will be considered in designing therapies for advanced and multi-therapy resistant cancer.

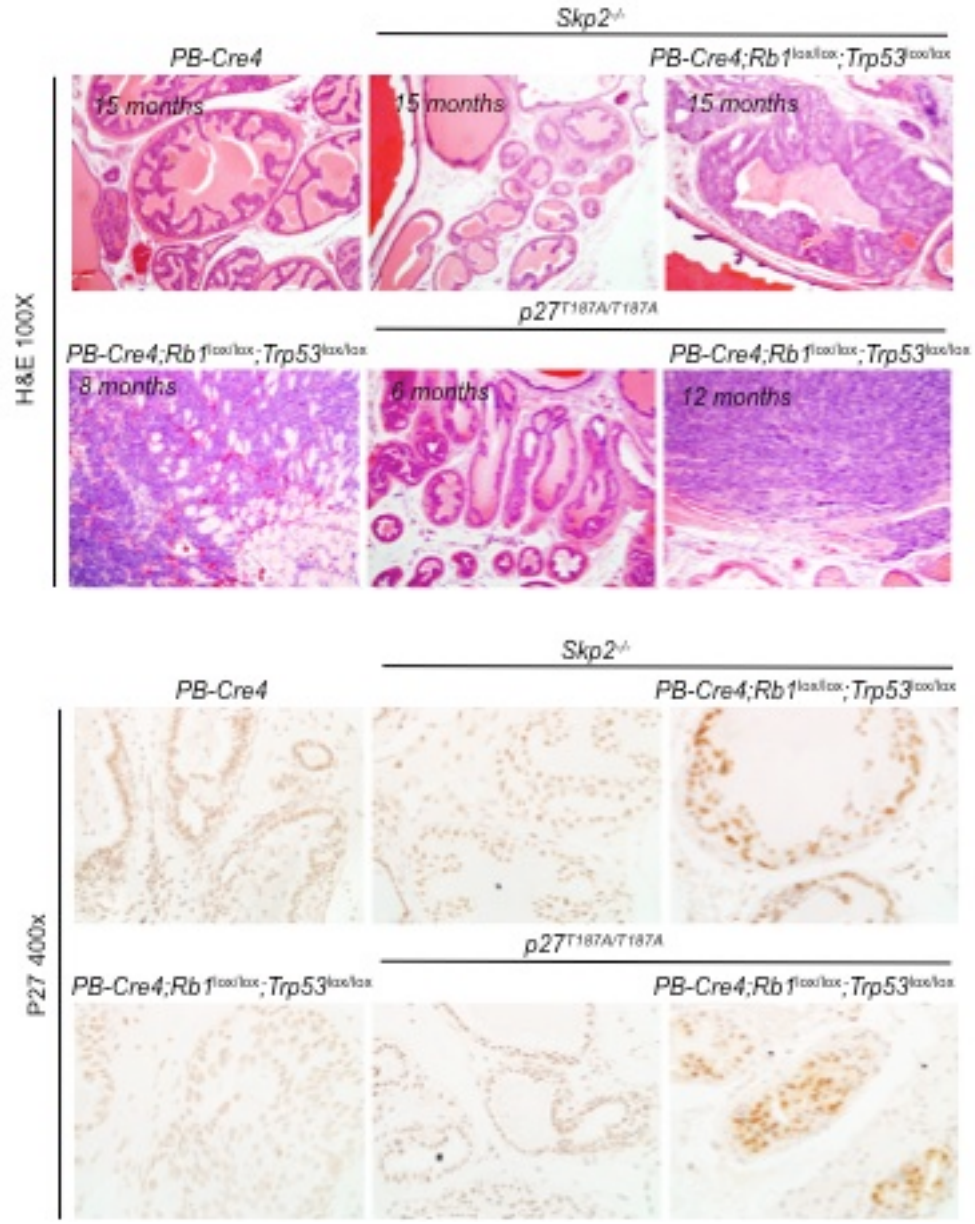

Figure 2 Sections of prostates from mice of six genotypes at the indicated ages stained with hematoxylin and eosin (H&E), anti-p27.

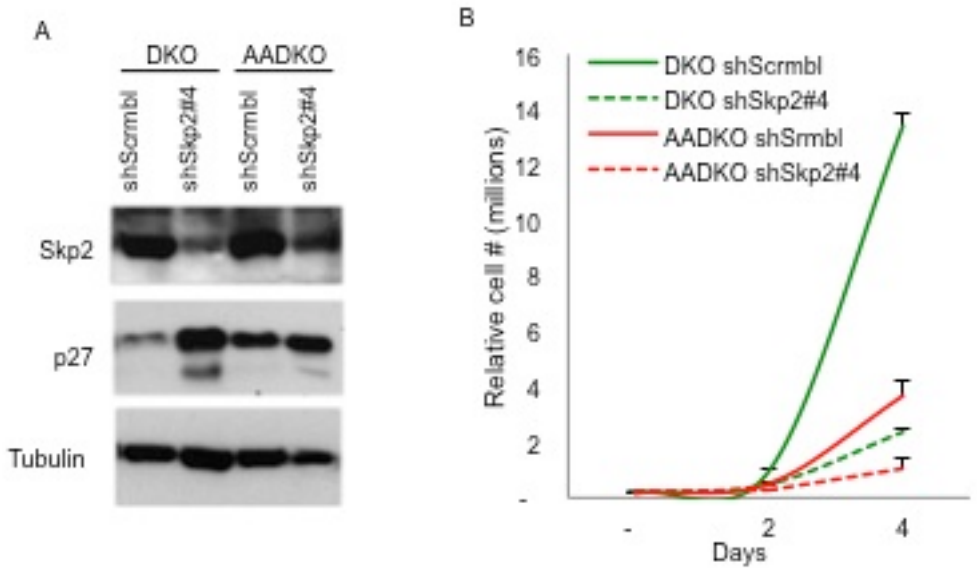

Figure 3 (A) Western blots of isolated tumor cell lines from 7-8 month old DKO and AADKO mice (B) Cell proliferation of the indicated cell lines is measured by counting cell numbers.

Task 3. To determine the role of Skp2 in prostate stem cell and prostate cancer stem cell compartments (Timeline 1-12 months).

I will focus this task this year and dissect the role of Skp2 in prostate stem cell and prostate cancer stem cell compartments as proposed in the project narrative.

KEY RESEARCH ACCOMPLISHMENTS:

1. Identification of KPC1 as a p53 target gene.
2. Identification of p27 as an antitumor safeguard following p53 inactivation, which usually masked by the presence of Skp2.
3. Identification additional antitumor mechanisms that remain effective when both pRb and p53, two major tumor suppressors, are genetically inactivated.
4. Generation of further impact in the form of new antitumor strategies for advance prostate cancers and cancers arising from other tissues.

CONCLUSION:

pRb and p53 are the two of the best known tumor suppressor proteins. They play key roles in provide most and best of the cells' intrinsic antitumor mechanisms, such as proliferation

arrest, cellular senescence, and apoptosis. pRb and p53 are frequently inactivated in cancer. Reactivating pRb and p53 is a major goal of anticancer strategies. While many investigators have studied and successfully demonstrated the importance of pRb and p53 in tumor suppression by deleting Rb1 or TP53 to establish various mouse tumor models, very few cancer researchers have attempted to inhibit tumorigenesis in models that mutate both pRb and p53. Indeed, it was not known whether pRb and p53 doubly deficient tumorigenesis could be blocked without resorting to severe measures that are incompatible with normal cell proliferation. This research demonstrated unequivocally that pRb and p53 doubly deficient tumorigenesis can be completely blocked (at least in the mouse prostate). Moreover, this research has achieved this by deleting a molecule that can be targeted without causing major defects in cell proliferation and mouse development. Thus, in this work, I have identified a vulnerability of pRb and p53 doubly deficient tumor cells, that can potentially be exploited therapeutically. In addition this study provides a cause for optimism, by showing that we can anticipate finding therapeutic strategies that are effective against highly aggressive cancers, such as those lacking RB1 and TP53.
Clearly more work will be needed to find drugs that target Skp2.

In order to fully understand the function of Skp2 in tumorigenesis, we are going to take advantage of our prostate tumor cell lines isolated from our DKO and AADKO mouse model and further characterize the differences between these cell lines regarding to anaerobic glycolysis and EMT, which will benefit the design strategies for targeting Skp2 in cancer treatment in the future.

PUBLICATIONS, ABSTRACTS, AND PRESENTATIONS:

Manuscripts submitted for publication during the period covered by this report resulting from this project.

1. Peer-Reviewed Scientific Journals*:* **Hongling Zhao**, Frederick Bauzon, Hao Fu, Zhonglei Lu, Jinhua Cui, Keiko Nakayama, Keiich I. Nakayama, Joseph Locker, and Liang Zhu "Skp2 deletion unmasks a p27 safeguard that blocks tumorigenesis in the absence of pRb and p53 tumor suppressors" Cancer Cell 2013 Nov 11;24(5):645-59.

2. Abstracts: Submitted abstract for **"**Cell Symposium, Hallmarks of Cancer: Asia, November 9-11, 2-14-Beijing, China" Please see appendices for detail

INVENTIONS, PATENTS AND LICENSES: Nothing to report

REPORTABLE OUTCOMES: Nothing to report

OTHER ACHIEVEMENTS:

Because of the research I have done supported by this award, I was selected as a recipient of the Dennis Shields Postdoctoral Research Prizes in 2014. Please see appendices for detail.

Opportunities for training and professional development:

1. Cancer center seminar, departmental weekly working in progress and journal club give me opportunities to developmental presentation skills and group discussion, which broaden my knowledge.

2. Discussion of project with my mentor, Dr. Liang Zhu, on daily basis, which make sure the project is on the right track and solves problems in the experiments.

3. Learning project thinking flow and grant writing with my mentor, Dr. Liang Zhu, and preparation for grant writing and develop my own academic career.

REFERENCES:

1. Marino, S., Vooijs, M., van Der Gulden, H., Jonkers, J., and Berns, A. (2000). Induction of medulloblastomas in p53-null mutant mice by somatic inactivation of Rb in the external granular layer cells of the cerebellum. Genes Dev. 14, 994– 1004.

2. Meuwissen, R., Linn, S.C., Linnoila, R.I., Zevenhoven, J., Mooi, W.J., and Berns, A. (2003). Induction of small cell lung cancer by somatic inactivation of both Trp53 and Rb1 in a conditional mouse model. Cancer Cell 4, 181–189.

3. Walkley, C.R., Qudsi, R., Sankaran, V.G., Perry, J.A., Gostissa, M., Roth, S.I., Rodda, S.J., Snay, E., Dunning, P., Fahey, F.H., et al. (2008). Conditional mouse osteosarcoma, dependent on p53 loss and potentiated by loss of Rb, mimics the human disease. Genes Dev. 22, 1662–1676.

4. Berman, S.D., Calo, E., Landman, A.S., Danielian, P.S., Miller, E.S., West, J.C., Fonhoue, B.D., Caron, A., Bronson, R., Bouxsein, M.L., et al. (2008). Metastatic osteosarcoma induced by inactivation of Rb and p53 in the osteoblast lineage. Proc. Natl. Acad. Sci. USA 105, 11851–11856.

5. Zhou, Z., Flesken-Nikitin, A., Corney, D.C., Wang, W., Goodrich, D.W., Roy-Burman, P., and Nikitin, A.Y. (2006). Synergy of p53 and Rb deficiency in a conditional mouse model for metastatic prostate cancer. Cancer Res. 66, 7889–7898.

6. Flesken-Nikitin, A., Choi, K.C., Eng, J.P., Shmidt, E.N., and Nikitin, A.Y. (2003). Induction of carcinogenesis by concurrent inactivation of p53 and Rb1 in the mouse ovarian surface epithelium. Cancer Res. 63, 3459–3463.

7. Jiang, Z., Deng, T., Jones, R., Li, H., Herschkowitz, J.I., Liu, J.C., Weigman, V.J., Tsao, M.S., Lane, T.F., Perou, C.M., and Zacksenhaus, E. (2010). Rb deletion in mouse mammary progenitors induces luminal-B or basal-like/ EMT tumor subtypes depending on p53 status. J. Clin. Invest. 120, 3296–3309.

8. McClendon, A.K., Dean, J.L., Ertel, A., Fu, Z., Rivadeneira, D.B., Reed, C.A., Bourgo, R.J., Witkiewicz, A., Addya, S., Mayhew, C.N., et al. (2011). RB and p53 cooperate to prevent liver tumorigenesis in response to tissue damage. Gastroenterology 141, 1439–1450.

9. Zhou, Z., Flesken-Nikitin, A., and Nikitin, A.Y. (2007). Prostate cancer associated with p53 and Rb deficiency arises from the stem/progenitor cell-enriched proximal region of prostatic ducts. Cancer Res. 67, 5683-5690.

10. Chia-Hsin Chan, Chien-Feng Li, et al (2012). The Skp2-SCF E3 ligase regulates Akt ubiquitination, glycolysis, Herceptin sensitivity and tumorigenesis. Cell 149, 1098-1111.

11. Inuzuka H, Gao D, Finley LW, Yang W, Wan L, et al (2012). Acetylation-dependent regulation of Skp2 function. Cell. 150, 179-193

APPENDICES:

Cancer Cell
Article

Skp2 Deletion Unmasks a p27 Safeguard that Blocks Tumorigenesis in the Absence of pRb and p53 Tumor Suppressors

Hongling Zhao,[1,2,3,4] Frederick Bauzon,[1,2,3,4] Hao Fu,[1,2,3,4] Zhonglei Lu,[1,2,3,4] Jinhua Cui,[1,2,3,4] Keiko Nakayama,[5] Keiich I. Nakayama,[6] Joseph Locker,[7] and Liang Zhu[1,2,3,4,*]
[1]Department of Developmental and Molecular Biology, Albert Einstein College of Medicine, Bronx, NY 10461, USA
[2]Department of Medicine, Albert Einstein College of Medicine, Bronx, NY 10461, USA
[3]Albert Einstein Cancer Center, Albert Einstein College of Medicine, Bronx, NY 10461, USA
[4]Marion Bessin Liver Research Center, Albert Einstein College of Medicine, Bronx, NY 10461, USA
[5]Division of Cell Proliferation, Advanced Research and Translational Medicine, Tohoku University Graduate School of Medicine, Sendai 980-8575, Japan
[6]Department of Molecular and Cellular Biology, Medical Institute of Bioregulation, Kyushu University, Fukuoka 812-8582, Japan
[7]Department of Pathology, University of Pittsburgh School of Medicine, Pittsburgh, PA 15261, USA
*Correspondence: liang.zhu@einstein.yu.edu
http://dx.doi.org/10.1016/j.ccr.2013.09.021

SUMMARY

pRb and p53 are two major tumor suppressors. Here, we found that p53 activates expression of Pirh2 and KPC1, two of the three ubiquitin ligases for p27. Loss of p53 in the absence of Skp2, the third ubiquitin ligase for p27, shrinks the cellular pool of p27 ubiquitin ligases to accumulate p27 protein. In the absence of pRb and p53, p27 was unable to inhibit DNA synthesis in spite of its abundance, but could inhibit division of cells that maintain DNA replication with rereplication. This mechanism blocked pRb/p53 doubly deficient pituitary and prostate tumorigenesis lastingly coexistent with bromodeoxyuridine-labeling neoplastic lesions, revealing an unconventional cancer cell vulnerability when pRb and p53 are inactivated.

INTRODUCTION

The prototype tumor suppressor retinoblastoma protein (pRb) is a transducer between the cell's environment and gene expression machinery (Burkhart and Sage, 2008). Fully active pRb recruits chromatin-modifying proteins to the promoters of E2F target genes to repress genes for DNA replication, which can be sufficiently potent and permanent to induce cellular senescence (Chicas et al., 2010). Upstream, pRb is regulated by phosphorylation by cyclin-dependent kinases (CDKs). Various signaling pathways can activate expression of relevant CDKs and cyclin-dependent kinase inhibitors (CKIs) to inactivate pRb (such as by cyclin D1/Cdk4 to induce tumorigenesis) or to activate pRb (such as by p16Ink4A to induce senescence) (Sherr, 2012).

The other major tumor suppressor, p53, is activated by oncogenic stress, such as the loss of pRb, directly or indirectly via Arf (Sherr, 2012). Activated p53 switches on its target genes to induce cell-cycle arrest, senescence, and apoptosis to safeguard against tumorigenesis.

In experimental settings, most of the cell's intrinsic antitumor mechanisms seem to function via p53, pRb, or both. Indeed, combined deletion of *Rb1* (encoding pRb) and *Trp53* (encoding p53) is very effective in inducing tumors in a wide spectrum of tissues in mice. Clinically, inactivation of both pRb and p53 is frequent in various cancers and may explain, in large part, why cancers are difficult to treat. In recent studies, investigators have discovered that deleting *Skp2*, a subunit of the Skp1, Cullin1, F-box protein complex, Cullin-Ring ubiquitin ligase 1 (SCF CRL1) E3 ubiquitin ligase, can induce apoptosis to block

Significance

Because pRb and p53 together are responsible for most antitumor mechanisms, their combined loss is frequent in cancers and explains in large part why cancers are difficult to treat. We discovered that deleting *Skp2* in mice allowed a p27 safeguard to be activated by the loss of p53 and pRb to block the otherwise aggressive tumorigenesis. This block of tumorigenesis lasted well into mouse old age. A counterintuitive feature of this block is that DNA synthesis persisted in the blocked neoplastic cells before they were eliminated by apoptosis. Thus, pRb/p53 doubly deficient tumors might be effectively treated by Skp2 inhibitors, but inhibition of DNA synthesis might not be a useful diagnostic criterion as traditionally practiced.

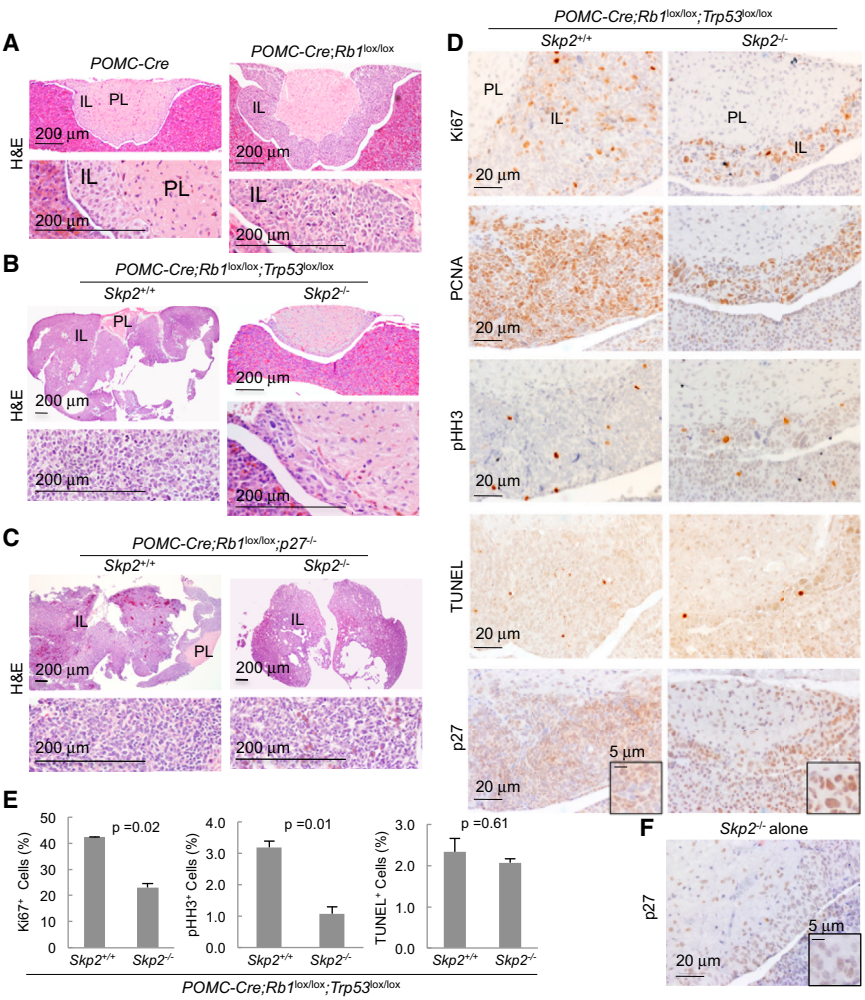

Figure 1. *Skp2* Deletion Blocks pRb/p53 Doubly Deficient, but Not pRb/p27 Doubly Deficient, Pituitary Tumorigenesis

(A–C) Hematoxylin and eosin (H&E)–stained sections of pituitary samples at 7 weeks of age. Higher-magnification views of the intermediate lobe (IL) are presented under lower-magnification ones. PL, posterior lobe.

(D) Pituitary sections of indicated genotypes were stained as indicated. For the *Skp2*$^{+/+}$;*POMC-Cre*;*Rb1*$^{lox/lox}$;*Trp53*$^{lox/lox}$ genotype, we selected pituitaries that were not deformed by macroscopic tumors. PCNA, proliferating cell nuclear antigen; pHH3, phosphohistone 3; TUNEL, terminal deoxynucleotidyl transferase deoxyuridine triphosphate nick-end labeling.

(E) Quantification of cells shown in (D) that stained positive with Ki67, pHH3, or TUNEL.

(F) A representative image of *Skp2*$^{-/-}$ pituitaries stained for p27.

Scale bars are as marked. Quantitative data are presented as averages ± SEM. Statistical analyses were carried out by Student's t test. See also Figure S1.

pRb-deficient pituitary tumorigenesis (Wang et al., 2010) or induce p53-independent senescence to block tumorigenesis in *Arf*$^{-/-}$ mice or *Pten*-deficient prostate (Lin et al., 2010). These two findings might have conformed to the existing paradigm that p53 is activated to inhibit pRb-deficient tumorigenesis, and, vice versa, that pRb is activated to inhibit p53-deficient tumorigenesis, when Skp2 is absent. *Skp2* deletion, however, was found not to block tumorigenesis by *N*-ethyl-*N*-nitrosourea (Wang et al., 2010) or by Myc-driven lymphomagenesis (Old et al., 2010).

In this study, we sought to determine whether combined loss of pRb and p53 would leave cells defenseless against tumorigenesis in the absence of Skp2.

RESULTS

Skp2 Deletion Blocks pRb/p53 Doubly Deficient Pituitary Tumorigenesis

Deleting *Rb1* using *POMC-Cre* was sufficient to induce melanotroph tumorigenesis across the entire intermediate lobe (IL) in the pituitary (Figure 1A), whereas deleting *Trp53* did not do so (Figure S1A available online). Combined deletion of *Rb1* and *Trp53* greatly accelerated IL tumorigenesis (Figure 1B), demonstrating the safeguarding role of p53 following loss of *Rb1*. Remarkably, *Skp2* deletion still blocked this tumorigenesis (Figure 1B). In comparison, *p27* knockout (KO) induced IL hyperplasia (Fero et al., 1996; Kiyokawa et al., 1996; Nakayama et al., 1996) (Figure S1B) and accelerated pRb-deficient IL tumorigenesis to an extent similar to deletion of *Trp53*, but *Skp2* was dispensable in this context (Figure 1C).

Surprisingly, although the Skp2KO ILs did not develop tumors following co-deletion of *Rb1* and *Trp53* in them, they appeared to contain as much of the proliferation markers Ki67 and proliferating cell nuclear antigen (PCNA) as the Skp2 wild-type (WT), pRb/p53 doubly deficient ILs, which were undergoing rapid tumorigenesis (Figure 1D). Quantification of Ki67-positive cells on a percentage basis showed a reduction of about or less than twofold, but this finding was statistically significant (Figure 1E). In the same samples, the mitotic marker phosphohistone 3 (pHH3) was reduced threefold, suggesting a more significant inhibition in cell division (Figures 1D and 1E). Consistent with the substantial presence of proliferation markers, senescence-associated β-galactosidase (SA-β-gal) staining was negative in *Skp2*$^{-/-}$;*POMC-Cre*;*Rb1*$^{lox/lox}$;*Trp53*$^{lox/lox}$ IL (data not shown). Apoptosis was similarly infrequent in these two genotypes as measured by terminal deoxynucleotidyl transferase deoxyuridine triphosphate nick-end labeling (TUNEL) staining (Figures 1D and 1E), demonstrating that, indeed, p53 functioned to induce apoptosis in *Rb1*-deficient pituitary tumorigenesis in the absence of *Skp2* (Wang et al., 2010). Thus, the complete blocking of the highly accelerated tumorigenesis coexisted, unexpectedly, with abundant proliferation markers (also see Figure S1C).

Another unexpected finding was that *Skp2*$^{-/-}$;*POMC-Cre*;*Rb1*$^{lox/lox}$;*Trp53*$^{lox/lox}$ melanotrophs contained more p27 protein

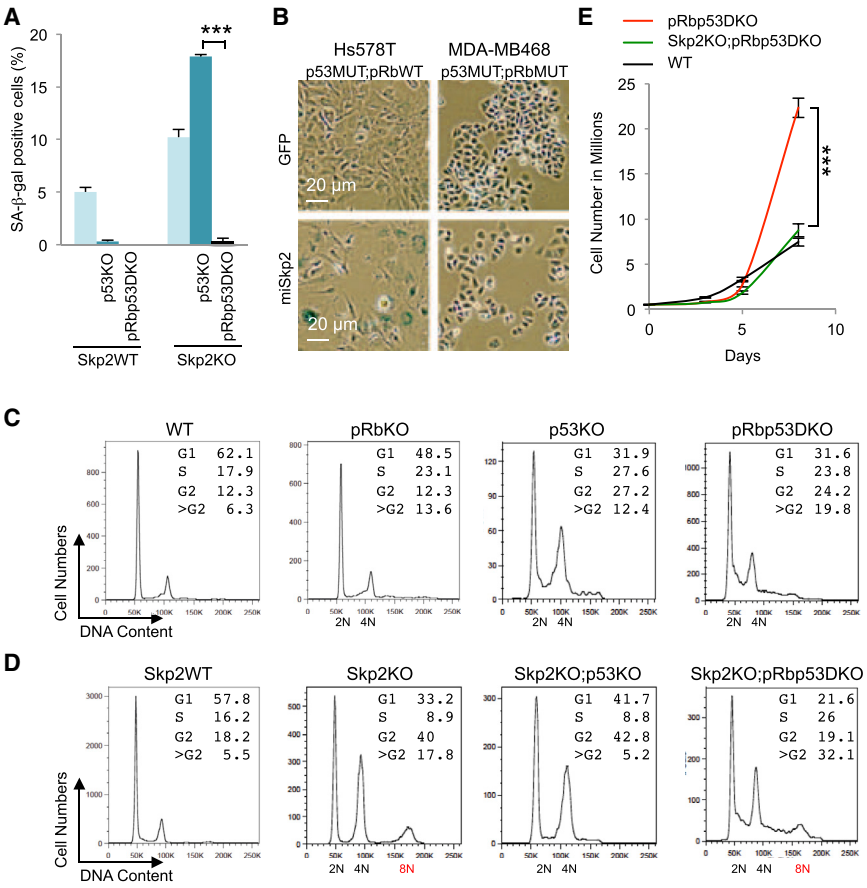

Figure 2. *Skp2/Rb1/Trp53* Triply Deficient Mouse Embryo Fibroblasts Show Higher DNA Replication and Rereplication, Accumulation at 8N, and Proliferation Speed of Wild-Type Mouse Embryo Fibroblasts

(A) Quantification of senescence-associated β-galactosidase (SA-β-gal) marker in mouse embryo fibroblasts (MEFs) of the indicated genotypes. DKO, double-knockout; KO, knockout.

(B) Human breast cancer cell lines with known pRb and p53 status (as indicated) were transduced with lentiviruses expressing green fluorescent protein (GFP) or miRNA hairpins targeting Skp2 (miSkp2). Five days after transduction, the same number of cells were plated. SA-β-gal staining was performed 3 days later.

(C and D) DNA content assessed by fluorescence-activated cell sorting (FACS) analysis of MEFs with the indicated genotypes. WT, wild type.

(E) Cell proliferation of the indicated MEFs is measured by counting cell numbers.

Quantitative data are presented as averages ± SEM. Statistical analyses were carried out by Student's t test. ***$p < 0.002$. FACS analysis results are representative of three experiments. See also Figure S2.

than *Skp2*$^{-/-}$ melanotrophs (Figures 1D and 1F; Figure S1C). This finding was controlled with staining of *p27*$^{-/-}$ pituitary (Figure S1D). p27 accumulated in the nuclei, and p27-abundant nuclei were larger, suggesting accumulation of more DNA.

Taken together, these results provide indications that, in the absence of Skp2, codeletion of *Rb1* and *Trp53* could further increase p27 protein levels, resembling a safeguard response, but that this high-level p27 is unable to inhibit expression of proliferation markers and induce senescence in the absence of pRb and p53. Nevertheless, the highly accelerated tumorigenesis was blocked.

Deleting *Trp53* in Skp2KO Mouse Embryo Fibroblasts Activates a pRb Safeguard to Induce Senescence

To further investigate the above-described unexpected findings, we generated mouse embryo fibroblasts (MEFs) of the same genotypes to study how *Skp2* deletion blocked pRb/p53 doubly deficient tumorigenesis. We used adeno-Cre to delete *Trp53*, *Rb1*, or both in MEFs controlled by parallel infection with adenovirus expressing green fluorescent protein (adeno-GFP). To simplify the text, we hereinafter refer to the various MEFs as p53KO, double-knockout pRbp53DKO, or Skp2KO; pRbp53DKO, for example.

Inactivation of p53 can immortalize Skp2WT MEFs but, to the contrary, it induces senescence in Skp2KO MEFs (Lin et al., 2010). In Figures 2A and S2A and 2B, we show, as measured by SA-β-gal staining, that Skp2WT;p53KO MEFs were prevented from senescence but that Skp2KO;p53KO MEFs senesced more than Skp2KO MEFs. To study how p53KO paradoxically induced more senescence in Skp2KO MEFs, and to determine whether combined deletion of *Rb1* would disable the senescence, we deleted *Rb1* in Skp2KO;p53KO MEFs (resulting in Skp2KO;pRbp53DKO MEFs) and prevented senescence (Figure 2A). To model therapeutic inhibition of Skp2, we performed Skp2 knockdown in the human breast cancer cell lines Hs578T and HCC1143, which contain functional pRb but are deficient for p53, and MDA-MB468 and BT549, which are deficient for both pRb and p53. Two tandem microRNA 30 (miR30)-based hairpins targeting Skp2 effectively reduced Skp2 protein and increased p27 protein in these cell lines (Sun et al., 2006) (Figure S2C). SA-β-gal staining revealed senescence in Hs578T cells, but not in MDA-MB468 cells, following Skp2 knockdown (Figures 2B and S2D). Thus, inactivation of p53 and Skp2 together activated a pRb safeguard to induce senescence. With additional loss of pRb, this line of antitumor defense is disabled, consistent with the abundant presence of proliferation markers in *Skp2*$^{-/-}$;*POMC-Cre*;*Rb1*$^{lox/lox}$;*Trp53*$^{lox/lox}$ IL.

Deleting *Trp53* and *Rb1* Induces DNA Rereplication

Notably, although the Skp2KO;pRbp53DKO genotype disabled senescence in MEFs and induced proliferation markers in IL, it induced no tumorigenesis. We subjected MEFs of relevant genotypes to fluorescence-activated cell sorting (FACS) analysis to study this unusual phenotype. As expected, deletion of *Rb1* or *Trp53* increased S phase cells (DNA content between 2N and 4N) and G_2 phase cells (4N) (Figure 2C).

Unexpectedly, deletion of *Rb1* or *Trp53* also generated more cells with DNA content larger than 4N (>G_2). Combined deletion of *Rb1* and *Trp53* increased this population to 20% (Figure 2C). The continuous distribution of the larger DNA content indicated DNA rereplication, which is defined as refiring of certain DNA replication origins before the entire set of chromosomes was fully duplicated (Arias and Walter, 2007). These findings reveal that pRb inhibits DNA rereplication and p53 safeguards against it. Notably, though combined loss of pRb and p53 did not synergistically increase S phase cells, it did for DNA rereplication (Figure 2C). Thus, a significant portion of elevated DNA synthesis activity during tumorigenesis following loss of pRb and p53 might be in the form of rereplication.

Codeleting *Trp53* and *Rb1* in Skp2KO Mouse Embryo Fibroblasts Induces Accumulation of DNA Rereplicating Cells by Mitotic Entry Delay

Consistent with previous reports that increased p27 in Skp2KO MEFs inhibited mitotic cyclin-Cdk (Nakayama et al., 2004), Skp2KO MEFs showed an increased G_2 population and an 8N peak. There was no accumulation of cells between 4N and 8N (Figure 2D), however. This profile indicates no DNA rereplication (as defined above), but the fully duplicated chromosomes failed to segregate into daughter cells before they were fully duplicated again.

Deletion of *Trp53* in Skp2KO MEFs, which induced senescence in them (Figure 2A), induced less DNA rereplication than p53KO MEFs (Figures 2C and 2D). Because pRb was activated in Skp2KO;p53KO MEFs to induce senescence (Figure 2A), a more active pRb might have inhibited DNA rereplication as well. Deletion of *Trp53* also abolished the 8N peak, suggesting that a more active pRb also blocked chromosome reduplication, likely due to the inhibition of DNA synthesis.

Skp2KO;pRbp53DKO MEFs, which were prevented from senescence, showed more S phase cells and DNA rereplication than Skp2KO;p53KO MEFs with return of the 8N peak, resulting in a total of 32% cells with DNA content larger than 4N (Figure 2D). This profile, together with the events leading to it, suggests that Skp2KO;pRbp53DKO allowed DNA rereplication to generate cells with more than 4N DNA content, and these cells gradually accumulated to an 8N peak. We further found that pHH3-positive cells were reduced from 1.13% in pRbp53DKO MEFs to 0.69% in Skp2KO;pRbp53DKO MEFs. These findings indicate the presence of a mitotic entry delay and are consistent with the significant decrease in pHH3-positive cells in *Skp2*$^{-/-}$;*POMC-Cre*;*Rb1*$^{lox/lox}$;*Trp53*$^{lox/lox}$ ILs (Figure 1D), whereas increased S phase and DNA rereplication explains the abundant presence of Ki67-positive and PCNA-positive cells (Figures 1D and 1E).

We counted cells to determine actual proliferation. We found that Skp2KO;pRbp53DKO MEFs proliferated at the speed of WT MEFs, despite much larger S phase populations. pRbp53DKO MEFs, despite S phase size similar to Skp2KO;pRbp53DKO MEFs, proliferated much faster than the latter, resulting in about threefold more cells at day 8 (Figure 2E). This difference in cell numbers resembled the tumorigenic potentials of these two genotypes in the pituitary. Similarly, human breast cancer cell lines MDA-MB468 and BT549 (mimicking pRbp53DKO) proliferated much faster than MDA-MB468-miSkp2 and BT549-miSkp2 (mimicking Skp2KO;pRbp53DKO), although the latter did not senesce (Figure 2B; Figures S2D and S2E).

These MEF studies modeled findings from the pituitary and provide insights into the unusual phenotypes of the Skp2KO;pRbp53DKO genotype. Chromosome separation failure restricted actual cell proliferation, whereas DNA rereplication sustained the presence of abundant proliferation markers.

p53 Loss Induces a p27 Safeguard

We next determined the molecular mechanisms for the phenotypes of Skp2KO;pRbp53DKO MEFs. Our finding that p27 protein levels were higher in *Skp2*$^{-/-}$;*POMC-Cre*;*Rb1*$^{lox/lox}$;*Trp53*$^{lox/lox}$ IL than in *Skp2*$^{-/-}$ IL (Figures 1D and 1F) suggested an elevation of a p27 safeguard by combined deletion of *Rb1* and *Trp53*. We performed western blot analysis to determine whether p27 protein levels in Skp2KO;pRbp53DKO MEFs also mimicked those in the pituitary. As expected, Skp2KO MEFs contained more p27 protein than Skp2WT MEFs (Figure 3A, lanes 1 and 3) (Nakayama et al., 2000). Combined deletion of *Rb1* and *Trp53* did not change p27 protein levels in Skp2WT MEFs (Figure 3A, lanes 1 and 2), but further increased p27 protein levels in Skp2KO MEFs (Figure 3A, lanes 3 and 4). Thus, MEFs again mimicked IL.

We investigated whether deleting *Rb1* or *Trp53* alone could further increase p27 protein in Skp2KO MEFs. We found that Skp2KO;p53KO MEFs (Figure 3A, lane 12), but not Skp2KO;pRbKO MEFs (Figure 3A, lane 8), contained increased p27 protein levels. Because p53 is gradually activated with passages of cultured MEFs (Figure S3A, lanes 1 and 2), deletion of *Trp53* in late-passage Skp2KO MEFs induced higher amounts of p27 (Figure S3A, lanes 6 and 7). Deletion of *Rb1* activated p53 in early-passage MEFs (Figure S3A, lane 3), which might explain why combined deletion of *Trp53* and *Rb1* induced the most p27 protein in Skp2KO MEFs (Figure 3A).

These findings explain why deletion of *Trp53* in Skp2KO MEFs induced higher levels of p27, which inhibits S phase cyclin-dependent kinases. Consequently, pRb is less phosphorylated and therefore more active. The activated pRb in turn inhibits DNA synthesis to induce senescence. This role of pRb as a transducer between inhibition of S phase cyclin-dependent kinases and inhibition of DNA synthesis is essential because Skp2KO;pRbp53DKO MEFs resumed DNA synthesis and failed to senesce. In comparison, because Skp2KO;pRbp53DKO MEFs are delayed for mitotic entry, the inhibition of mitotic cyclin-dependent kinases (by high p27 levels) can inhibit mitotic entry without activated pRb.

To determine the functional significance of the high p27 in blocking mitotic entry, we knocked down p27 in Skp2KO;pRbp53DKO MEFs with two p27-targeting hairpins (Figure S3B). Short hairpin 2 (sh2) reduced p27 protein in Skp2KO;pRbp53DKO MEFs to below that in Skp2WT;pRbp53DKO MEFs, abolished the 8N peak and reduced 4N to 8N cells (Figure S3C), and increased proliferation of Skp2KO;pRbp53DKO MEFs faster than Skp2WT;pRbp53DKO MEFs (Figure S3D). sh1 knocked down p27 to a lesser degree and reduced 4N to 8N cells and increased proliferation to a smaller extent. Thus, accumulation of 4N to 8N DNA content and inhibition of proliferation of pRbp53DKO MEFs by *Skp2* deletion was highly dependent on high p27 protein levels. When we used a

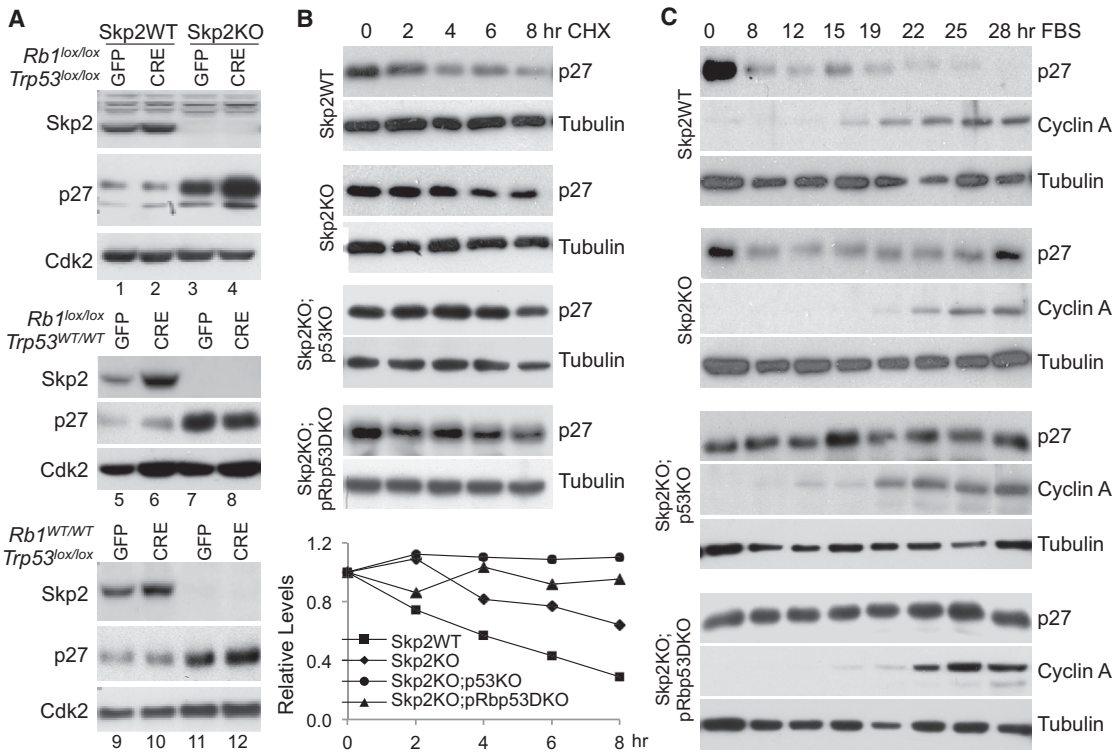

Figure 3. Deletion of *Trp53* Triggers Further Stabilization of p27 Protein in Skp2KO Mouse Embryo Fibroblasts

(A) Western blot analysis of indicated proteins in mouse embryo fibroblasts (MEFs) of indicated genotypes transduced in parallel by adenovirus expressing green fluorescent protein (adeno-GFP) or adeno-Cre (CRE). KO, knockout; WT, wild type.

(B) Cell extracts were prepared from MEFs of indicated genotypes at the indicated time points following the addition of cycloheximide (CHX), and the amounts of p27 protein were measured by western blot analysis in comparison to tubulin. p27 protein level quantification is presented under the gels.

(C) Cell extracts were prepared from MEFs of indicated genotypes at indicated time points after being cultured in serum-containing media following serum starvation for 3 days. The p27 protein level was determined by western blot analysis. The cyclin A protein level is shown to indicate cell-cycle progression, and the tubulin level is shown to indicate loading amounts. FBS, fetal bovine serum.

See also Figure S3.

cytomegalovirus (CMV) promoter to overexpress p27 in Skp2WT;pRbp53DKO MEFs (Figure S3E), p27 protein levels increased less than twofold (Figure S3F), cells did not accumulate 8N DNA content (data not shown), and proliferation rates were only slightly reduced (Figure S3G), suggesting that p27 protein degradation is the major regulator of p27 levels and functions in Skp2WT;pRbp53DKO MEFs.

The further increases in p27 protein levels were not associated with increases in p27 mRNA levels (Figure S3H), but they were associated with more stable p27 proteins (Figure 3B). This finding indicated that Skp2-independent p27 degradation mechanisms were reduced by deletion of *Trp53* in Skp2KO MEFs. That deletion of *Trp53* did not induce higher p27 in Skp2WT MEFs suggests that Skp2 possesses sufficient p27 degradation activity to compensate for reduction in other p27 protein degradation mechanisms.

In addition to Skp2, p27 is ubiquitinated by KPC1 and Pirh2 ubiquitin ligases, which function primarily at early time points of cell-cycle entry (Hattori et al., 2007; Kamura et al., 2004). We used serum starvation release to determine whether *Trp53* deletion affected p27 protein degradation within this time window. Figure 3C shows that Skp2KO did not prevent reduction of p27 protein levels at early time points (hours 8, 12, and 15), but prevented its further reduction at hours 22 and 25. *Trp53* deletion or combined *Trp53* and *Rb1* deletion did not affect the kinetics of p27 protein reduction in Skp2WT MEFs (data not shown), but prevented p27 protein reduction at hours 8, 12, and 15 in Skp2KO MEFs (Figure 3C). This finding suggests that *Trp53* deletion impaired the ability of KPC1 and/or Pirh2 to degrade p27.

Interestingly, Pirh2 was previously identified as a p53 target gene (Leng et al., 2003). We used the Transcription Regulatory Element Database (Xuan et al., 2005) to study whether the KPC1 gene promoter contains a p53 binding site, which is a ten-nucleotide consensus sequence repeated once with a spacer of 0 to 13 nucleotides (el-Deiry et al., 1992; Wei et al., 2006) (Figure S4A). The promoter of p21, a canonical p53 target gene, contains a p53 binding site with a matched first half and one mismatched second half. (We call it a 0,1 site.) The Pirh2 promoter contains a 0,1 site, and the KPC1 promoter contains a 1,1 site (Figure S4B). Skp2 and p27 promoters contain a 1,2 site and a 2,1 site, respectively.

The chromatin immunoprecipitation (ChIP) experiments shown in Figure 4A demonstrate that activation of p53 in WT MEFs by doxorubicin (DOX) stimulated recruitment of p53 to the promoters of p21, Pirh2, and KPC1, but not Skp2 and

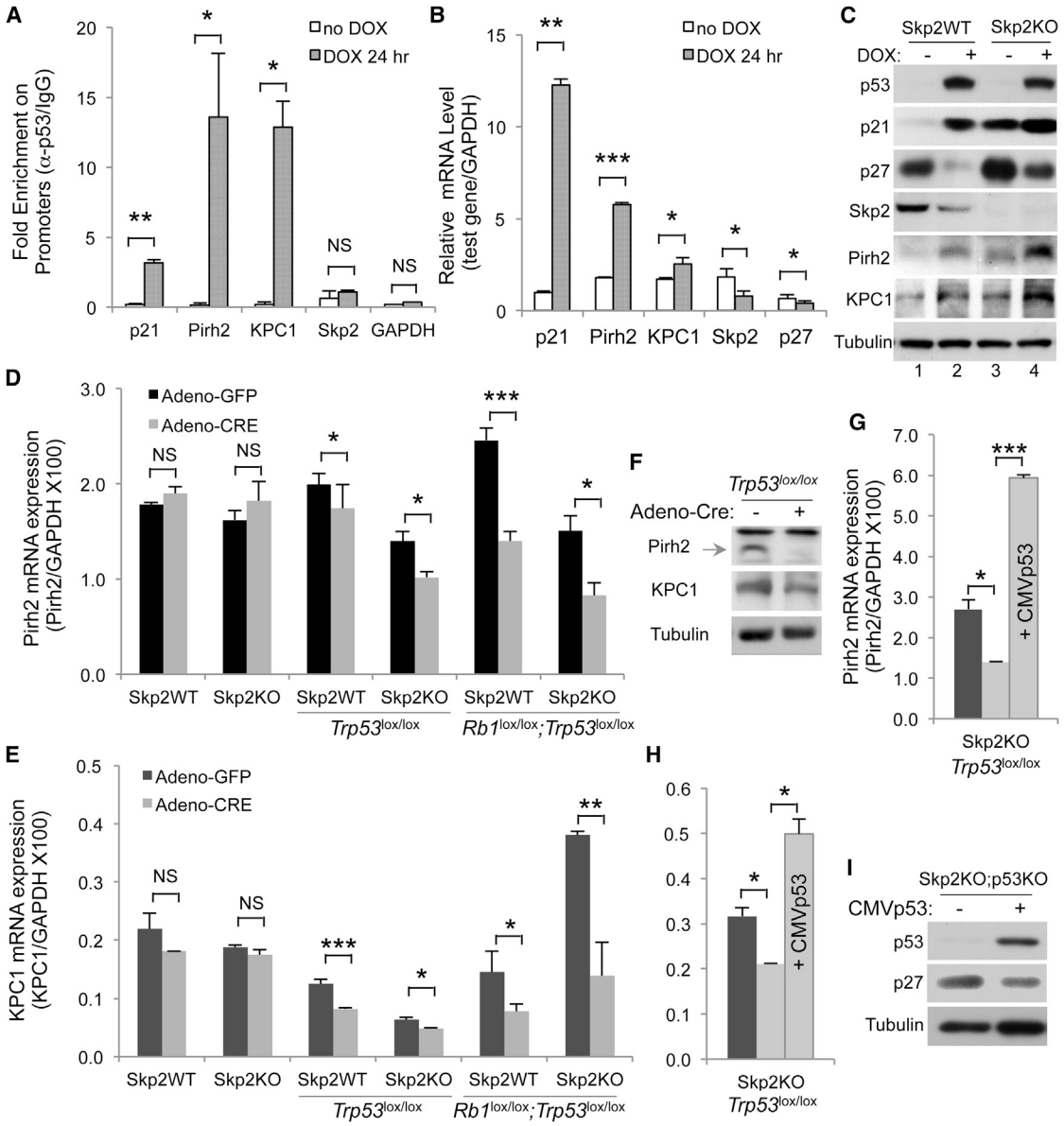

Figure 4. p27 Ubiquitin Ligases Pirh2 and KPC1 Are p53 Target Genes

(A) The results of chromatin immunoprecipitation assays with anti-p53 and control immunoglobulin G (IgG) following doxorubicin (DOX) treatment of wild-type (WT) mouse embryo fibroblasts (MEFs). Fold enrichment (anti-p53/IgG) for the indicated promoters is presented. GAPDH, glyceraldehyde 3-phosphate dehydrogenase.

(B) RT-quantitative PCR (RT-qPCR) of the indicated genes in WT MEFs following DOX treatment, normalized with GAPDH.

(C) Western blot of the indicated MEFs following treatment with DOX as in (B). KO, knockout.

(D and E) Expression of Pirh2 (D) and KPC1 (E) in MEFs transduced in parallel by adeno-GFP and adeno-Cre. Values were normalized with GAPDH.

(F) Western blots of Pirh2 and KPC1 before and after deletion of *Trp53*.

(G and H) Same as (D) and (E) with an additional sample in which p53 was ectopically expressed, as marked inside the bars. CMV, cytomegalovirus.

(I) Western blots of Skp2KO;p53KO MEFs without or with ectopic p53 expression.

Quantitative data are presented as average ± SEM. Student's t test was used for statistical analysis. *p < 0.05; **p < 0.01; ***p < 0.002; NS, p > 0.05. See also Figure S4.

glyceraldehyde 3-phosphate dehydrogenase. In agreement with the ChIP results, the expression levels of Pirh2 and KPC1 were stimulated by DOX, although to smaller degrees than the stimulation of p21 expression; but DOX did not stimulate expression of Skp2 or p27 (Figure 4B). The western blots show that p53, p21, Pirh2, and KPC1 proteins were increased, and that Skp2 protein was decreased, by DOX treatment (Figure 4C). We then confirmed that DOX counterintuitively decreased p27 protein levels (Figure 4C, lanes 1 and 2). Notably, DOX also reduced p27 protein levels in Skp2KO MEFs (Figure 4C, lanes 3 and 4). Thus, strong p53 activation and acute *Trp53* deletion have opposite effects on p27 protein levels. We explored the possibility that

these changes in protein levels were due to changes in cell-cycle profiles by DOX. We found that under the conditions we used, DOX did not dramatically change cell-cycle profiles of WT or Skp2KO MEFs (Figure S4C).

We next determined the effects of *Trp53* deletion on the expression of Pirh2 and KPC1. Figures 4D and 4E show that *Trp53* deletion alone or with *Rb1* reduced mRNA levels of Pirh2 and KPC1 in both Skp2WT and Skp2KO MEFs. The effects of *Trp53* deletion were smaller than *Trp53* and *Rb1* codeletion, likely because p53 was not highly activated in cultured MEFs before *Rb1* was deleted (Figures 3A and S3A). The western blots show that Pirh2 and KPC1 protein levels also decreased following deletion of *Trp53* (Figure 4F). Skp2 expression was not reduced following *Trp53* deletion or codeletion with *Rb1* (Figure S4D). When we reexpressed p53 in Skp2KO;p53KO MEFs, expression of Pirh2 and KPC1 increased (Figures 4G and 4H) and p27 protein levels decreased (Figure 4I). These results suggest that the combined reduction in Pirh2 and KPC1 expression shrinks the pool of the ubiquitin ligases for p27 further in Skp2KO;p53KO MEFs and therefore further increases p27 protein accumulation.

Knockdown of Pirh2 or KPC1 can increase p27 protein in various human and mouse cells (Hattori et al., 2007; Kamura et al., 2004). For our study, we ectopically expressed Pirh2 and KPC1 in Skp2KO;pRbp53DKO MEFs to determine their negative effects on high p27 levels. Although we succeeded in increasing Pirh2 levels by expression of CMV-huPirh2, expression of CMV-huKPC1 increased KPC1 protein levels only slightly in these MEFs (Figure S4E). Under these conditions, expression of Pirh2, KPC1, or both reproducibly decreased p27 protein levels, reduced 4N to 8N cells, and increased proliferation (Figures S4E–S4G), but all these effects were smaller than those observed with p27 knockdown (Figures S3B–S3D). In MDA-MB468 and BT549 breast cancer cell lines with Skp2 knockdown (mimicking Skp2KO;pRbp53DKO MEFs), expression of CMV-huPirh2 and CMV-huKPC1 also increased proliferation, most effectively in BT549 cells (Figures S4H–S4K). These results confirmed the functions of Pirh2 and KPC1 in promoting p27 degradation and proliferation, but the extent of their overexpression and phenotypes is cell type–dependent.

Skp2 Deletion Blocks pRb/p53 Doubly Deficient Prostate Tumorigenesis

We sought to determine whether our findings regarding the pituitary and MEFs were applicable to another tissue. Although *Rb1* deletion is sufficient to induce pituitary tumorigenesis, it requires combined deletion of *Trp53* to induce tumorigenesis in the brain (Marino et al., 2000), lung (Meuwissen et al., 2003), bone (Walkley et al., 2008; Berman et al., 2008), prostate (Zhou et al., 2006), ovary (Flesken-Nikitin et al., 2003), breast (Jiang et al., 2010), and liver (McClendon et al., 2011), suggesting that these tissues may mount a stronger p53 safeguard following *Rb1* deletion. We studied the prostate. *PB-Cre4*;*Rb1*$^{lox/lox}$;*Trp53*$^{lox/lox}$ mice developed rapid and invasive prostate cancer (Zhou et al., 2006). The prostate tumors became lethal from 6 months and killed all hosts (n = 58) within 1 year (Figure 5A) (Zhou et al., 2006). In contrast, all *Skp2*$^{-/-}$;*PB-Cre4*;*Rb1*$^{lox/lox}$;*Trp53*$^{lox/lox}$ mice (n = 32) survived, as WT mice did, for the 19-month period (Figure 5A). Pathological diagnoses for these two cohorts are shown in Figure 5B. Prostatic intraepithelial neoplasias (PINs) were divided into four grades (Park et al., 2002). At 3 to 4 months, PINs developed in both cohorts (also see Figure S5A). PINs in *PB-Cre4*;*Rb1*$^{lox/lox}$;*Trp53*$^{lox/lox}$ mice were of higher grades and quickly progressed to invasive carcinoma (Figures 5B and 5C; Figure S5B) and gross tumors during the 5- to 7-month period, when 20 of 42 mice died. In the 8- to 9-month period, most tumors had become macroscopic and all mice died by the end of the ninth month. In contrast, PINs in *Skp2*$^{-/-}$;*PB-Cre4*;*Rb1*$^{lox/lox}$;*Trp53*$^{lox/lox}$ mice never progressed beyond the PIN stage in a total of 26 mice examined, 6 of which were examined at 15 to 22 months.

Figures 5D and 5F show that PIN lesions in *Skp2*$^{-/-}$;*PB-Cre4*;*Rb1*$^{lox/lox}$;*Trp53*$^{lox/lox}$ mice contained higher levels of p27, as measured by immunohistochemical and western blot analysis of dissected ventral and anterior lobes, than they did in *Skp2*$^{-/-}$ glands. Nuclei expressing higher p27 protein levels were larger. PCNA expression was also high in *Skp2*$^{-/-}$;*PB-Cre4*;*Rb1*$^{lox/lox}$;*Trp53*$^{lox/lox}$ PINs (Figure 5E).

We used Ki67 staining to compare the proliferation status of PINs. Normal glands of WT and *Skp2*$^{-/-}$ mice contained few Ki67-positive cells, and PINs contained more of them (Figures 6A and 6B). Remarkably, the abundance of Ki67-positive cells was similar between PINs in *PB-Cre4;Rb1*$^{lox/lox}$;*Trp53*$^{lox/lox}$ mice and PINs in *Skp2*$^{-/-}$;*PB-Cre4*;Rb1$^{lox/lox}$;*Trp53*$^{lox/lox}$ mice. The presence of pHH3, on the other hand, was significantly reduced from 2.23% to 1.26% (Figures 6C and 6F). If PINs in *Skp2*$^{-/-}$;*PB-Cre4*;*Rb1*$^{lox/lox}$;*Trp53*$^{lox/lox}$ mice were undergoing DNA rereplication with mitotic entry block, as demonstrated by the MEF model of this genotype (Figure 2D), their nuclei should accumulate larger amounts of DNA. We used 4′,6-diamidino-2-phenylindole (DAPI) and Feulgen stains to study this and found that nuclei in PINs of the *Skp2*$^{-/-}$;*PB-Cre4*;*Rb1*$^{lox/lox}$;*Trp53*$^{lox/lox}$ genotype contained significantly more DAPI and Feulgen staining than the other three genotypes (Figures 6D, 6E, and 6G).

Thus, the ability of *Skp2* deletion to block pRb/p53 doubly deficient tumorigenesis and the mechanisms underlying this block were essentially the same in the prostate and the pituitary, as modeled in MEFs.

Lifelong Block in Bromodeoxyuridine Labeling Prostatic Intraepithelial Neoplasias

We next addressed the possibility that S phase Skp2KO;pRbp53DKO MEFs (as determined by DNA content) and proliferating *Skp2*$^{-/-}$;*PB-Cre4*;*Rb1*$^{lox/lox}$;*Trp53*$^{lox/lox}$ PINs (as determined by Ki67 and PCNA expression) might not actually be synthesizing DNA as reasons for slow proliferation of MEFs and absence of tumorigenesis for PINs. Cells containing more than 4N DNA content due to rereplication were found to cease DNA synthesis by activating p53-dependent checkpoints (Zhu et al., 2004). If cells of the Skp2KO;pRbp53DKO genotype had ceased DNA synthesis, a mechanism to inhibit DNA synthesis (and therefore tumorigenesis) following rereplication in the absence of pRb and p53 would be implicated.

We first addressed this issue by analyzing bromodeoxyuridine (BrdU)-labeled (30 minutes) Skp2KO;pRbp53DKO MEFs in parallel with WT and pRbp53DKO MEFs. For these three genotypes, cells defined as being in S phase by DNA content on the *x*-axis (positions indicated by yellow arrows) were shifted upward to become BrdU-positive on the *y*-axis (positions indicated by red

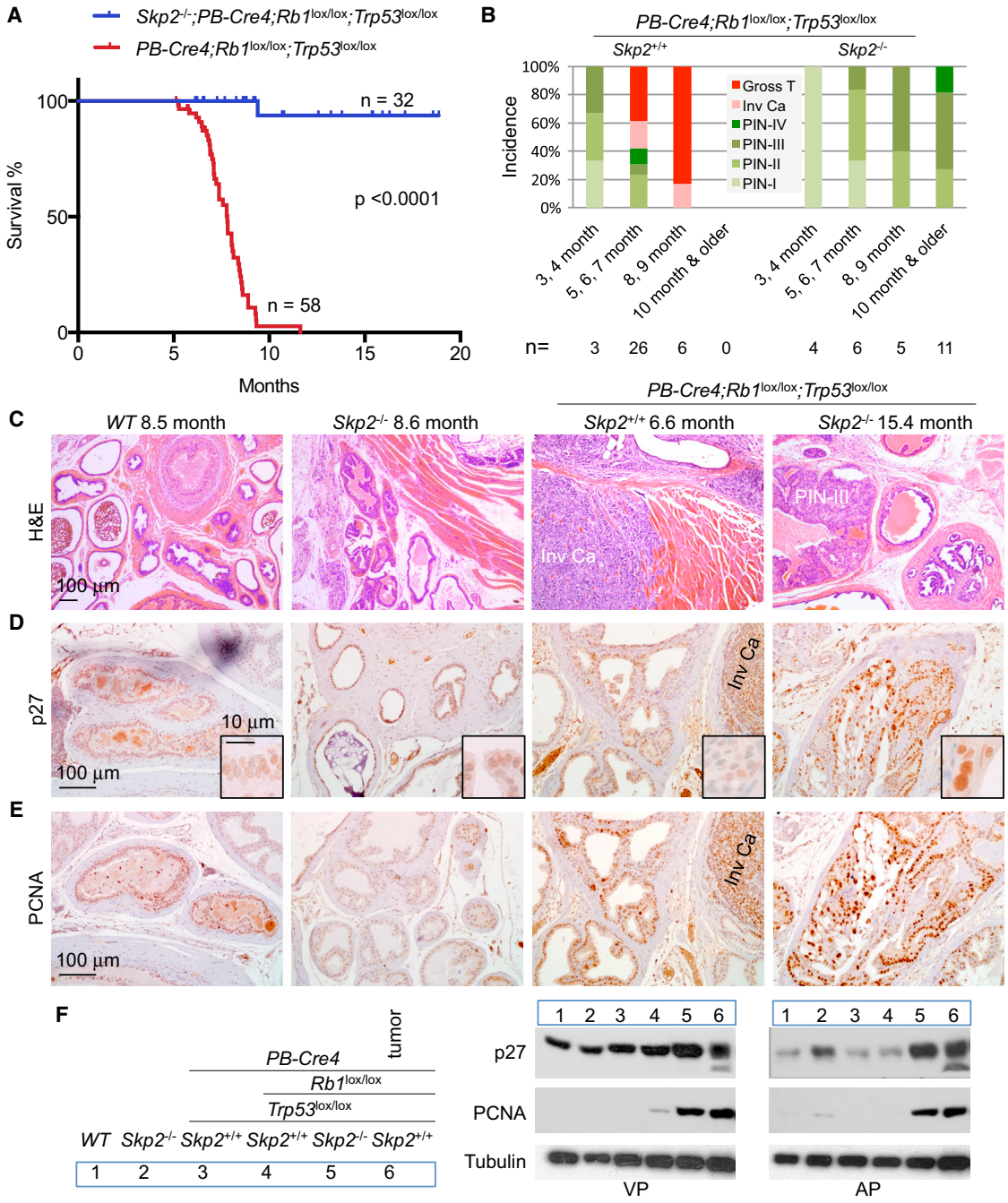

Figure 5. Deletion of *Skp2* Blocks pRb/p53 Doubly Deficient Prostate Tumorigenesis inside Prostatic Intraepithelial Neoplasia Stages

(A) Kaplan-Meier survival analysis of two cohorts of mice with indicated genotypes. One *Skp2*$^{-/-}$;*PB-Cre4*;*Rb1*$^{lox/lox}$;*Trp53*$^{lox/lox}$ mouse died from fighting at 9.4 months without prostate tumors.

(B) Pathological diagnoses of prostate lesions in mice of indicated genotypes in four age groups. Each prostate was serially sectioned and the most advanced lesions were the diagnoses. PIN, prostatic intraepithelial neoplasia.

(C–E) Sections of prostates from mice of four genotypes at the indicated ages stained with hematoxylin and eosin (H&E) (C), anti-p27 (D), and anti-proliferating cell nuclear antigen (anti-PCNA; E). Invasive carcinoma (Inv Ca) and a PIN-III lesion are marked. WT, wild type.

(F) Western blots of isolated ventral prostates (VPs) and anterior prostates (APs) from 3- to 4-month-old mice. A macroscopic tumor was included as marked. See also Figure S5.

arrows), demonstrating that they were actively synthesizing DNA during the labeling period (Figure 7A). The ratios of BrdU-positive cells versus BrdU-negative cells were similar between pRbp53DKO MEFs and Skp2KO;pRbp53DKO MEFs (2.0 and 1.7, respectively), but much higher than the ratio of WT MEFs (0.3), consistent with the results shown in Figures 2C and 2D.

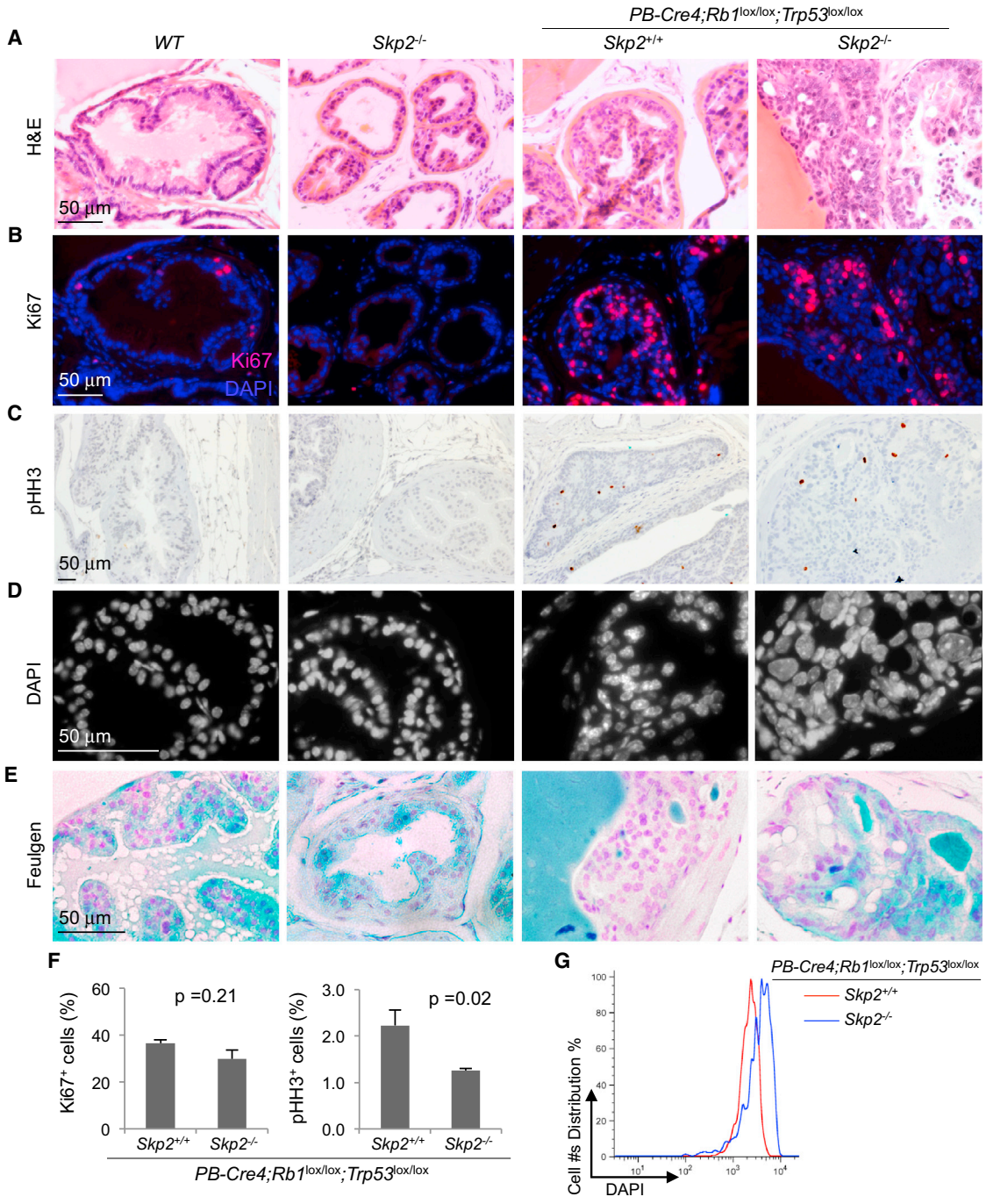

Figure 6. Comparisons of Proliferation Markers and Nuclear Sizes in Prostate of the Indicated Genotypes

(A–E) Sections of prostates from mice with indicated genotypes at same ages as those shown in Figure 5C were stained with hematoxylin and eosin (H&E; A), anti-Ki67 (B), anti-phosphohistone 3 (anti-pHH3) (C), 4′,6-diamidino-2-phenylindole (DAPI; D), and Feulgen (E).

(F) Quantification of Ki67-positive cells and pHH3-positive cells from (B) and (C), respectively.

(G) DAPI-stained slides were quantified using an iCys Research Imaging Cytometer and iCys Cytometric Analysis Software.

Quantitative data are presented as averages ± SEM. Student's t test was used for statistical analysis.

Cells containing more than 4N DNA content were also largely BrdU-positive. The ratios of BrdU-positive cells with more than 4N DNA to BrdU-negative cells with more than 4N DNA were 5.7 for both pRbp53DKO and Skp2KO;pRbp53DKO MEFs, but 1.1 for WT MEFs. Thus, there was no indication of a pRb- and p53-independent inhibitory checkpoint effect on DNA synthesis in response to DNA rereplication.

We labeled mice with BrdU (2 hr) to determine whether prostate PINs were actively synthesizing DNA. We found numerous BrdU-positive cells in PINs of both genotypes, although labeling

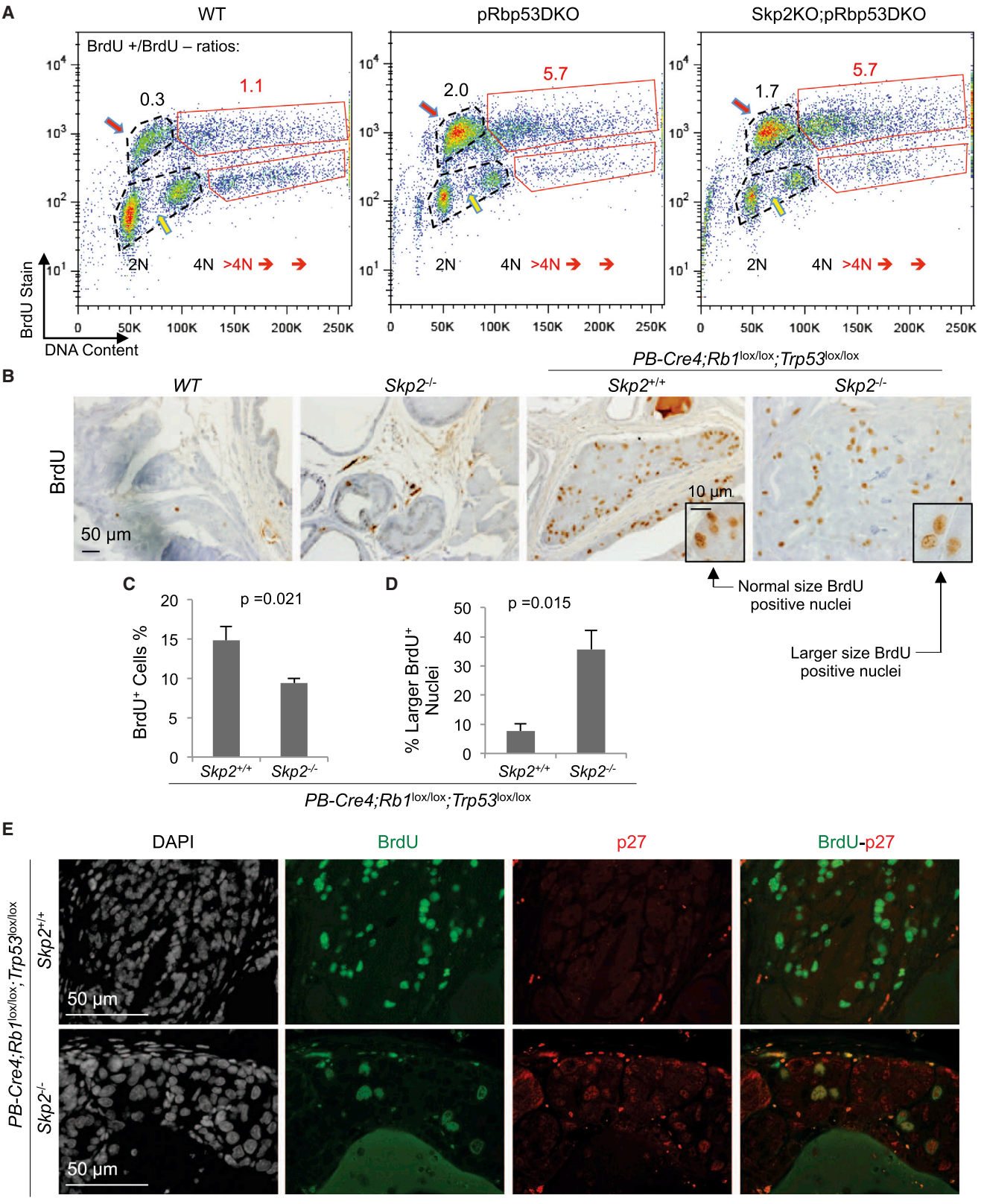

(legend on next page)

frequency was reduced from 14.85% to 9.39% by the deletion of *Skp2* (Figures 7B and 7C). Although this was a statistically significant reduction, it was less than twofold. We noticed that BrdU-positive nuclei in *Skp2*$^{-/-}$;*PB-Cre4*;*Rb1*$^{lox/lox}$;*Trp53*$^{lox/lox}$ PINs were larger than those in *PB-Cre4*;*Rb1*$^{lox/lox}$;*Trp53*$^{lox/lox}$ PINs (compare the two insets in Figure 7B). Figure 7D shows that 35.7% of BrdU-positive cells contained larger nuclei in *Skp2*$^{-/-}$;*PB-Cre4*;*Rb1*$^{lox/lox}$;*Trp53*$^{lox/lox}$ PINs, compared to 7.6% in *PB-Cre4*;*Rb1*$^{lox/lox}$;*Trp53*$^{lox/lox}$ PINs. These findings suggest that DNA synthesis activities in *Skp2*$^{-/-}$;*PB-Cre4*;*Rb1*$^{lox/lox}$;*Trp53*$^{lox/lox}$ PINs derived largely from DNA rereplication, explaining the presence of larger nuclei in them. Furthermore, BrdU-positive and larger nuclei also contained higher p27, as shown by double-staining for BrdU and p27 (Figure 7E).

The results discussed in this section solidify the salient feature of the *Skp2* deletion-mediated block of pRb/p53 doubly deficient tumorigenesis. In the absence of pRb and p53, deregulation of DNA replication in the form of rereplication persists in neoplastic lesions that are apparently blocked for life by higher levels of p27. Figure S6 shows more examples of BrdU-labeling PINs in four *Skp2*$^{-/-}$;*PB-Cre4*;*Rb1*$^{lox/lox}$;*Trp53*$^{lox/lox}$ mice ages 11 to 22 months.

Blocked Skp2KO;pRbp53DKO Prostatic Intraepithelial Neoplasia Cells Succumb to Apoptosis

Although pRb/p53 doubly deficient prostate tumorigenesis did not progress beyond PINs in *Skp2*$^{-/-}$ mice as old as 22 months, the PIN lesions persisted coexistent with active DNA synthesis. Although entry to mitosis was blocked, as indicated by significant reduction in pHH3-positive cells (Figures 6C and 6F; Figure S6), more than half of the pHH3-positive cells were in metaphase. Mitotic figures were also present in hematoxylin and eosin–stained sections of blocked PIN lesions. These features appeared inadequate to explain the lifelong block of pRb/p53 doubly deficient prostate tumorigenesis in *Skp2*$^{-/-}$ mice and would be compatible for selection of resistant cells.

To determine whether this block of tumorigenesis also involved cell elimination, we measured the rates of apoptosis in these PINs. TUNEL stain–positive cells were about 5.3% in pRbp53DKO PINs and increased to 8.4% in Skp2KO;pRbp53DKO PINs, which is not statistically significant (Figures 8A and 8D). Invasive carcinomas showed similar rates of apoptosis as measured by TUNEL staining. Detection of activated caspase 3 (aCasp3) yielded similar results. We next used nuclear condensation and fragmentation morphology (also called apoptotic bodies or pyknosis) to detect apoptosis (Figure 8B, inset a). We unexpectedly found that morphologically apoptotic cells were TUNEL-positive (Figure 8B, inset b) as well as TUNEL-negative (Figure 8B, inset c). Similarly, cells with condensed nuclei (by DAPI staining) were positive or negative for aCasp3 (Figure 8B, insets d and e). After we confirmed the ability of our TUNEL and aCasp3 staining to detect apoptosis by examining intestinal villi (Figure S7), we reevaluated apoptosis by combining TUNEL staining with morphological assessment. The results (Figures 8C and 8D) show that apoptosis rates remained similar with determination by TUNEL alone for DKO PINs, but increased twofold in invasive cancer and triple-knockout (TKO) PINs. Areas with as much as 20% apoptotic cells were frequently observed in TKO PINs. Figure 8C (black arrows in a, b, and c) indicates a typical stepwise process of late apoptosis leading to the elimination of the cell. The block of pRb/p53 doubly deficient prostate tumorigenesis in *Skp2*$^{-/-}$ mice therefore was not solely due to cytostatic mechanisms. Apoptotic elimination of blocked Skp2KO;pRbp53DKO PIN cells could contribute to the lifelong block of tumorigenesis by reducing the possibility for the emergence of resistant cells by, for example, epigenetically silencing p27 expression.

DISCUSSION

Tumorigenesis is a multistep process. Because of the cells' intrinsic antitumor safeguards, the first oncogenic events seldom succeed. pRb and p53 tumor suppressors are major effectors of antitumor safeguards and are therefore frequently inactivated in cancer. To learn how to treat cancers after all the antitumor mechanisms exemplified by pRb and p53 have been exhausted, we conducted the current study. To completely and irreversibly inactivate pRb and p53, we deleted the genes encoding them.

In this context, we discovered that deletion of *Skp2* unmasked a *Trp53* deletion-induced safeguard to elevate p27 protein levels. In the absence of Skp2, loss of activated p53 shrinks the pool of p27 ubiquitin ligases further by reducing expression of the p27 E3 ligases Pirh2 and KPC1 and therefore accumulates p27 protein further. This rise of p27 in Skp2KO;p53KO cells effectively inhibited the S phase to the extreme of cellular senescence. Critically, additional deletion of *Rb1* disabled this senescence antitumor mechanism. Not only DNA replication but also rereplication became uninhibitable, even in the presence of high levels of p27. These findings add a dramatic piece of evidence for the importance of keeping at least one of these two major tumor suppressors for the prevention and treatment of cancer.

Figure 7. Sustained Active DNA Synthesis in Skp2KO;pRbp53DKO Mouse Embryo Fibroblasts and in *Skp2*$^{-/-}$;*PB-Cre4*;*Rb1*$^{lox/lox}$;*Trp53*$^{lox/lox}$ Prostatic Intraepithelial Neoplasias

(A) Representative fluorescence-activated cell sorting analysis plots (from three experiments) of DNA content by propidium iodide staining and bromodeoxyuridine (BrdU) content by anti-BrdU staining. The numbers of BrdU-positive and BrdU-negative cells in the regular cell cycle were determined within the dotted black circles, and the ratios are indicated in black numbers above the circles. Numbers of cells with > 4N DNA contents were similarly analyzed with red boxes and red numbers. DKO, double-knockout; KO, knockout.

(B and C) Prostate sections from BrdU-injected mice with indicated genotypes were stained with BrdU (B), and quantification of BrdU-positive cells is shown in (C). WT, wild type.

(D) Quantification of normal-sized and larger BrdU-positive nuclei as portions of the entire BrdU-positive cell populations is shown.

(E) Prostate sections from BrdU-injected mice with indicated genotypes were stained with 4′,6-diamidino-2-phenylindole (DAPI), anti-BrdU and anti-p27. The *Skp2*$^{-/-}$;*PB-Cre4*;*Rb1*$^{lox/lox}$;*Trp53*$^{lox/lox}$ sample, which was taken from a 21.7-month-old mouse, shows persistence of prostatic intraepithelial neoplasia cells containing enlarged nuclei with high p27 and BrdU incorporation.

Quantitative data in (C) and (D) are presented as averages ± SEM. Student's t test was used for statistical analysis. See also Figure S6.

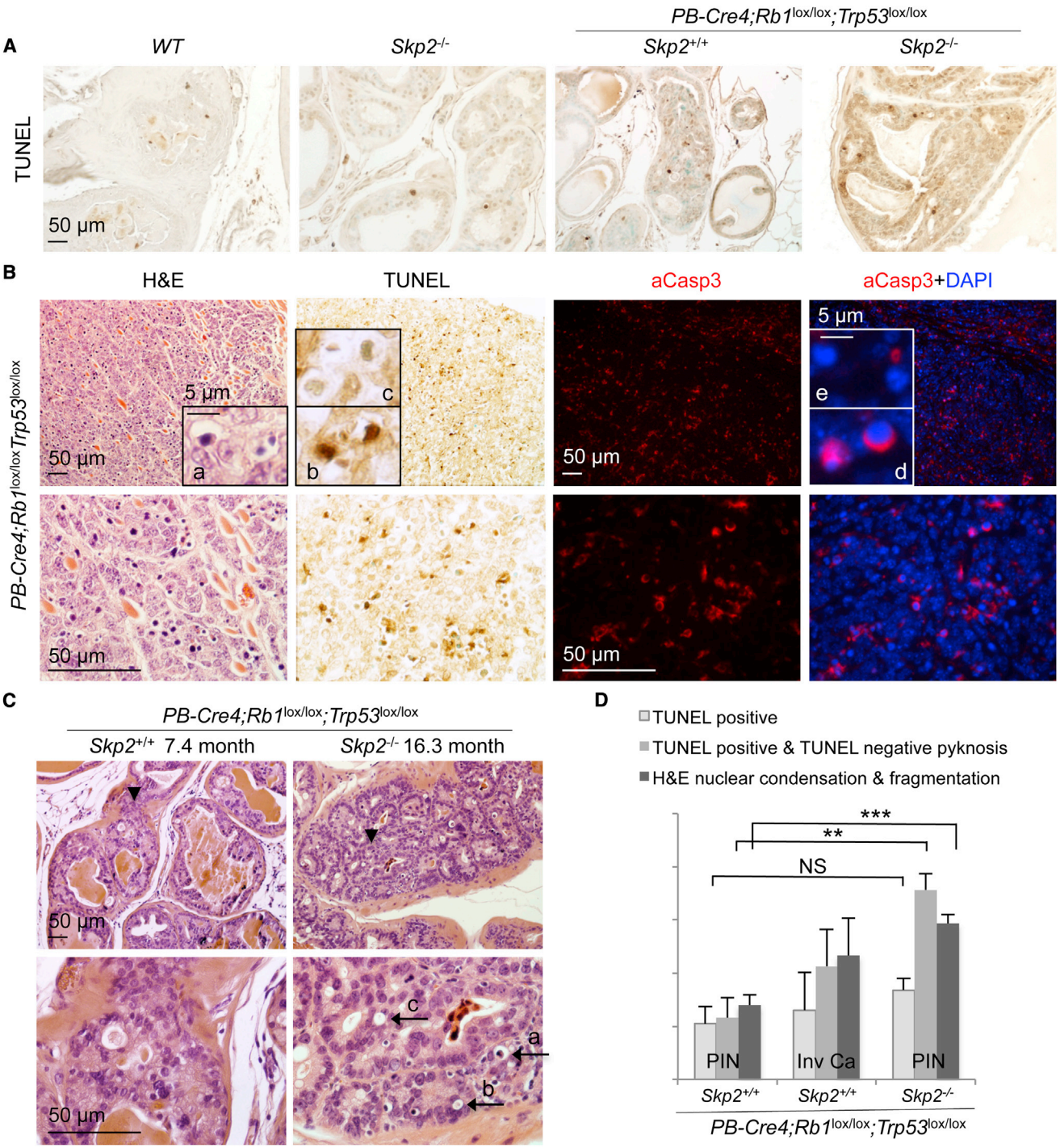

Figure 8. Blocked *Skp2*$^{-/-}$;*PB-Cre4;Rb1*$^{lox/lox}$;*Trp53*$^{lox/lox}$ Prostatic Intraepithelial Neoplastic Cells Succumb to Apoptosis

(A) Terminal deoxynucleotidyl transferase deoxyuridine triphosphate nick-end labeling (TUNEL) staining of prostate sections of the indicated genotypes. WT, wild type.

(B) Comparison of apoptosis detection by nuclear morphology (inset a), TUNEL stain (insets b and c), and activated caspase 3 (aCasp3) and 4′,6-diamidino-2-phenylindole (DAPI) costains (insets d and e) in a microscopic tumor. H&E, hematoxylin and eosin.

(C) Representative H&E-stained prostatic intraepithelial neoplasia (PIN) section of the indicated genotypes. Lower panels show higher-magnification views of areas indicated by black arrowheads in the corresponding upper panels. Black arrows indicate typical apoptotic morphologies as described in the text.

(D) Quantification of apoptosis rates in the indicated lesions by three different methods as marked.

Quantitative data are presented as averages ± SEM. Student's t test was used for statistical analysis. $^{**}p < 0.01$; $^{***}p < 0.002$; NS, $p > 0.05$.

See also Figure S7.

Unexpectedly, however, our study results consistently show that pRb/p53 doubly deficient prostate tumorigenesis in the absence of Skp2 was blocked lastingly. This unique coexistence of BrdU-labeling neoplastic lesions and a tumor-free life generated a counterintuitive preclinical model of complete block of tumorigenesis. In addition to revealing a vulnerability of pRb/p53 doubly deficient tumors, this model suggests an unconventional concept for the diagnosis, treatment, and management of the worst types of cancer. At the surface level, detection of abundant proliferation markers would immediately lead to the diagnosis of a more aggressive cancer carrying a poor prognosis, whereas in fact they could be lastingly blocked neoplastic lesions.

Up to now, tumor block has been associated with dramatic reduction of proliferation markers down to the extremes of cellular senescence. Although ostensibly elevated to block tumorigenesis, cellular senescence, the most studied safeguard, could also secrete cytokines and growth factors to promote tumorigenesis (Coppé et al., 2010; Krtolica et al., 2001; Kuilman and Peeper, 2009). Recent evidence shows that oncogenic Nras induced senescence in hepatocytes to induce liver cancer when the senescence cells were not cleared (Kang et al., 2011) and that DOX treated *Wnt1*-induced mammary tumors more effectively in the absence of p53 induced cellular senescence than in its presence (Jackson et al., 2012).

Persistent DNA rereplication could provide different ways to overcome tumor block and promote tumorigenesis. DNA rereplication is logically a source for gene amplification and genomic instability. On an ongoing basis, these changes can generate new mutations that inhibit p27 expression or promote p27 protein degradation and/or nuclear export to disable the block to pRb/p53 doubly deficient tumorigenesis. This scenario is expected to lead to rapid tumorigenesis because pRb and p53 are already inactivated. The fact that this scenario did not materialize up to the old age of 22 months of mouse life is surprising. It is possible, however, that this blocking mechanism for pRb/p53 doubly deficient tumorigenesis will delay tumor progression to the end stage only within the longer time frames of typical human cancers. On the other hand, our findings may suggest that Skp2 inactivation also stabilizes the genome via mechanisms yet to be identified. Further studies are required to determine the effects of inhibiting Skp2 on established tumors that are caused by inactivation of pRb and p53 but likely have undergone additional mutations during tumorigenesis.

Targeting Skp2 to treat cancer has already been actively pursued. The finding that *Skp2* deletion can induce p53-independent senescence (Lin et al., 2010) broadens its application to p53-deficient cancers, and a recent report has described a Skp2 inhibitor with this ability preclinically (Chan et al., 2013). Our present study broadens its application further to include pRb/p53 doubly deficient cancers and sheds more light on the design of Skp2 inhibitors. Protein degradation in the ubiquitin proteasome system (Ciechanover, 2005) proceeds via a set of hierarchic steps starting with target-specific polyubiquitination and ending in degradation of polyubiquitinated proteins in the proteasomes. For Skp2-mediated p27 ubiquitination and degradation, the most target-specific step is the interaction between $SCF(CRL1)^{Skp2/Cks1}$ with T187 phosphorylated p27, and an inhibitor blocking this interface has recently been identified (Wu et al., 2012). Inhibitors targeting the interaction between Skp2 and Skp1 in SCF E3 (Chan et al., 2013; Chen et al., 2008) blocks ubiquitination of p27 together with other substrates of SCF^{Skp2}, but they might spare substrates of SCF E3s employing other F-box proteins. Further upstream are inhibitors targeting the cullin subunit in all CRL E3 ligases (Soucy et al., 2009). Inhibitors of ubiquitin-conjugating enzymes (E2s) have also been identified. Targeting CDC34, which functions with CRLs, inhibited not only p27 ubiquitination but also a larger group of CRL substrates (Ceccarelli et al., 2011). Although the above-named inhibitors and their designs can all inhibit Skp2-mediated p27 ubiquitination with varying degrees of selectivity, they do not inhibit Pirh2 and KPC1, because they are not CRL-type E3s and do not depend on CDC34 as E2 for the ubiquitination of p27.

Proteasome inhibitors, by definition, do not target specific proteins or specific groups of proteins. Impressively, however, the proteasome inhibitor bortezomib was approved by the U.S. Food and Drug Administration and has demonstrated remarkable efficacy in treating multiple myeloma and mantle cell lymphoma. Stabilization of p27 might be an important mechanism for its therapeutic efficacy, although other effects caused by nonspecific accumulation of proteins might also be responsible, especially for its side effects. In this respect, the proteasome inhibitor argyrin A (Nickeleit et al., 2008) exhibited antitumor activities in a p27-dependent manner. Because argyrin A is a more specific proteasome inhibitor than bortezomib (Nickeleit et al., 2008), its intriguing effects could suggest that truly specific inhibition of proteasomes could indeed effectively treat cancer "specifically" through p27 stabilization. It will be important to determine whether this occurs because inhibiting proteasomes disabled the whole cellular pool of p27 E3s, including Skp2, Pirh2, KPC1, and likely others (Cao et al., 2011). Our study provides a basis for explaining why pan-inhibition of p27 degradation mechanisms would be more effective than specific inhibition of Skp2 for cancer treatment.

EXPERIMENTAL PROCEDURES

Mice

POMC-Cre mice (Balthasar et al., 2004), *PB-Cre4* mice (Wu et al., 2001), $Rb1^{lox/lox}$ mice (Sage et al., 2003), $Trp53^{lox/lox}$ mice (Jonkers et al., 2001), $Skp2^{+/-}$ mice (Nakayama et al., 2000), and $p27^{-/-}$ mice (Fero et al., 1996) have been described. *POMC-Cre* mice (Bradford B. Lowell Laboratory) were obtained on an FVB background, $Rb1^{lox/lox}$ mice (Tyler Jacks Laboratory) on a C57BL6J×129Sv background, $Trp53^{lox/lox}$ mice (National Cancer Institute (NCI) mouse repository) on an FVB×129 background, $Skp2^{-/-}$ mice on a C57BL6J×129Sv background, $p27^{-/-}$ mice (The Jackson Laboratory) on a C57BL6J background, and *PB-Cre4* mice (NCI mouse repository) on a C57BL6J×Cg background. Subsequent breeding did not select for or against any particular strain background. Testing genotypes were studied with control genotypes from littermates. Genotyping details are provided in the Supplemental Information. Animals were housed in the Albert Einstein College of Medicine animal facility. Mouse procedures were reviewed and approved by the Albert Einstein College of Medicine Animal Care Committee, conforming to accepted standards of humane animal care. Mouse pathological studies were conducted together with the Albert Einstein Cancer Center Mouse Pathology Core.

Mouse Embryo Fibroblasts, Human Breast Cancer Cell Lines, and Treatments

MEFs were prepared from embryonic day 13.5 embryos and cultured in Dulbecco's modified Eagle's medium (DMEM) containing 10% fetal bovine serum (FBS). Parallel infection with adeno-Cre or adeno-GFP were used to delete or

mock-delete *Rb1* or/and *Trp53* in MEFs containing floxed *Rb1* or/and floxed *Trp53*. Controls also included infection with adeno-Cre of MEFs without floxed *Rb1* or *Trp53*. Knockdown or overexpression was carried out by lentiviral transduction and drug selection with puromycin (catalog no. BP2956-100; Fisher Scientific) or blasticidin (catalog no. ant-bl-1; InvivoGen). DNA damage response was generated by treatment with 1 μM DOX (catalog no. BP2516-1; Fisher Scientific). Human breast cancer cell lines MDA-MB468, BT549, Hs578T, and HCC1143 (American Type Culture Collection) were cultured in RPMI 1640 medium containing 10% FBS, 1% penicillin/streptomycin, and 1% glutamine. Knockdown of Skp2 by miRNA was achieved by lentiviral transduction at near 100% efficiency. See Supplemental Information for details.

SA-β-gal Staining for Senescence, FACS Analysis for DNA Content and BrdU Labeling, and Cell Number Counting for Proliferation Determination

Standard protocols were used; details are in Supplemental Information.

Western Blot Analysis, RT-qPCR, and ChIP

Antibodies used for western blot analysis are Skp2 (H435), cyclin A (C-19), p21 (C-19), Pirh2 (FL261), PCNA (PC10), and Cdk2 (C-19) (all from Santa Cruz Biotechnology). Mouse anti-p27 antibody was obtained from BD Biosciences (catalog no. 610242), mouse anti-p53 antibody was obtained from Cell Signaling Technology (catalog no. 1C12) and Santa Cruz Biotechnology (SC-126). Antibody to α-tubulin was obtained from Sigma-Aldrich (catalog no. T6074). Antibody to KPC1 was described previously (Kamura et al., 2004). See Supplemental Information for experimental details and sequences of primers.

Cycloheximide Chase and Serum Starvation Release

For protein stability analysis, MEFs were plated into 60-mm dishes at 70%–80% confluence. Cycloheximide (CHX, catalog no. 239764; Calbiochem) was added at 50 μg/ml. At the indicated time points, cell extracts were prepared and western blotted. Quantification of protein levels was performed using ImageJ software (National Institutes of Health). Serum starvation of MEFs was carried out in 100-mm dishes at 80%–90% confluence in DMEM (1% penicillin/streptomycin, 1% glutamine) with 0.2% FBS. After 72 hr, cells were aliquoted into 60-mm dishes and restimulated with DMEM (1% penicillin/streptomycin, 1% glutamine) containing 10% FBS.

Immunohistochemistry, Immunofluorescence, TUNEL, and Bromodeoxyuridine Labeling

Antibodies included PCNA (catalog no. PC10; Santa Cruz Biotechnology), BrdU (catalog no. Ab-2; Calbiochem), pHH3 (Cell Signaling Technology), Ki67 (catalog no. SP6; Vector Laboratories), activated caspase 3 (catalog no. 9664S; Cell Signaling Technology), mouse anti-p27 antibody (catalog no. 610242; BD Biosciences), and rabbit anti-p27 antibody (catalog no. ab92741; Abcam). TUNEL staining was performed with an apoptosis detection kit (catalog no. S7100; EMD Millipore). For BrdU labeling, mice were injected with 0.4% BrdU (B5002; Sigma-Aldrich) at 25 μl/g body weight 2 hr before they were killed. See Supplemental Information for experiment details.

Statistical Analysis

In the survival analysis, differences in Kaplan-Meier survival curves were analyzed using a logrank test with GraphPad Prism 6 software (GraphPad Software). Differences in Ki67-, pHH3-, BrdU-, and TUNEL-positive cells between indicated samples were analyzed by Student's t test. P values < 0.05 were considered statistically significant.

SUPPLEMENTAL INFORMATION

Supplemental Information includes Supplemental Experimental procedures and seven figures and can be found with this article online at http://dx.doi.org/10.1016/j.ccr.2013.09.021.

AUTHOR CONTRIBUTIONS

H.Z. and L.Z. conceived and designed the research; H.Z., F.B., H.F., Z.L., and J.C. performed the research; K.I.N. and K.N. provided Skp2-mutant mice and KPC1 antibody; H.Z., J.L., and L.Z. analyzed the data; H.Z. and L.Z. wrote the manuscript; and all authors reviewed and approved the manuscript for publication.

ACKNOWLEDGMENTS

This work was supported by National Institutes of Health grants R01 CA127901 and R01 CA131421 (to L.Z.). The Albert Einstein Comprehensive Cancer Research Center (grant 5P30CA13330) and the Albert Einstein Comprehensive Liver Research Center (grant 5P30DK061153) provided core facility support. We thank Dr. Sarah Schweber of the Oncology Division for suggestions of human breast cancer cell lines and Dr. Jinghang Zhang of the Flow Cytometry Core Facility of the Albert Einstein Cancer Center for assistance in using iCys Research Imaging Cytometer and iCys Cytometric Analysis Software. H.Z. is a recipient of U.S. Department of Defense Prostate Cancer Research Program Postdoctoral Fellowship (PC121837), and L.Z. is a recipient of the Irma T. Hirschl Career Scientist Award.

Received: May 8, 2013
Revised: August 22, 2013
Accepted: September 30, 2013
Published: November 11, 2013

REFERENCES

Arias, E.E., and Walter, J.C. (2007). Strength in numbers: preventing rereplication via multiple mechanisms in eukaryotic cells. Genes Dev. *21*, 497–518.

Balthasar, N., Coppari, R., McMinn, J., Liu, S.M., Lee, C.E., Tang, V., Kenny, C.D., McGovern, R.A., Chua, S.C., Jr., Elmquist, J.K., and Lowell, B.B. (2004). Leptin receptor signaling in POMC neurons is required for normal body weight homeostasis. Neuron *42*, 983–991.

Berman, S.D., Calo, E., Landman, A.S., Danielian, P.S., Miller, E.S., West, J.C., Fonhoue, B.D., Caron, A., Bronson, R., Bouxsein, M.L., et al. (2008). Metastatic osteosarcoma induced by inactivation of Rb and p53 in the osteoblast lineage. Proc. Natl. Acad. Sci. USA *105*, 11851–11856.

Burkhart, D.L., and Sage, J. (2008). Cellular mechanisms of tumour suppression by the retinoblastoma gene. Nat. Rev. Cancer *8*, 671–682.

Cao, X., Xue, L., Han, L., Ma, L., Chen, T., and Tong, T. (2011). WW domain-containing E3 ubiquitin protein ligase 1 (WWP1) delays cellular senescence by promoting p27(Kip1) degradation in human diploid fibroblasts. J. Biol. Chem. *286*, 33447–33456.

Ceccarelli, D.F., Tang, X., Pelletier, B., Orlicky, S., Xie, W., Plantevin, V., Neculai, D., Chou, Y.C., Ogunjimi, A., Al-Hakim, A., et al. (2011). An allosteric inhibitor of the human Cdc34 ubiquitin-conjugating enzyme. Cell *145*, 1075–1087.

Chan, C.H., Morrow, J.K., Li, C.F., Gao, Y., Jin, G., Moten, A., Stagg, L.J., Ladbury, J.E., Cai, Z., Xu, D., et al. (2013). Pharmacological inactivation of Skp2 SCF ubiquitin ligase restricts cancer stem cell traits and cancer progression. Cell *154*, 556–568.

Chen, Q., Xie, W., Kuhn, D.J., Voorhees, P.M., Lopez-Girona, A., Mendy, D., Corral, L.G., Krenitsky, V.P., Xu, W., Moutouh-de Parseval, L., et al. (2008). Targeting the p27 E3 ligase SCF(Skp2) results in p27- and Skp2-mediated cell-cycle arrest and activation of autophagy. Blood *111*, 4690–4699.

Chicas, A., Wang, X., Zhang, C., McCurrach, M., Zhao, Z., Mert, O., Dickins, R.A., Narita, M., Zhang, M., and Lowe, S.W. (2010). Dissecting the unique role of the retinoblastoma tumor suppressor during cellular senescence. Cancer Cell *17*, 376–387.

Ciechanover, A. (2005). Proteolysis: from the lysosome to ubiquitin and the proteasome. Nat. Rev. Mol. Cell Biol. *6*, 79–87.

Coppé, J.P., Desprez, P.Y., Krtolica, A., and Campisi, J. (2010). The senescence-associated secretory phenotype: the dark side of tumor suppression. Annu. Rev. Pathol. *5*, 99–118.

el-Deiry, W.S., Kern, S.E., Pietenpol, J.A., Kinzler, K.W., and Vogelstein, B. (1992). Definition of a consensus binding site for p53. Nat. Genet. *1*, 45–49.

Fero, M.L., Rivkin, M., Tasch, M., Porter, P., Carow, C.E., Firpo, E., Polyak, K., Tsai, L.-H., Broudy, V., Perlmutter, R.M., et al. (1996). A syndrome of multiorgan hyperplasia with features of gigantism, tumorigenesis, and female sterility in p27(Kip1)-deficient mice. Cell *85*, 733–744.

Flesken-Nikitin, A., Choi, K.C., Eng, J.P., Shmidt, E.N., and Nikitin, A.Y. (2003). Induction of carcinogenesis by concurrent inactivation of *p53* and *Rb1* in the mouse ovarian surface epithelium. Cancer Res. *63*, 3459–3463.

Hattori, T., Isobe, T., Abe, K., Kikuchi, H., Kitagawa, K., Oda, T., Uchida, C., and Kitagawa, M. (2007). Pirh2 promotes ubiquitin-dependent degradation of the cyclin-dependent kinase inhibitor p27Kip1. Cancer Res. *67*, 10789–10795.

Jackson, J.G., Pant, V., Li, Q., Chang, L.L., Quintás-Cardama, A., Garza, D., Tavana, O., Yang, P., Manshouri, T., Li, Y., et al. (2012). p53-mediated senescence impairs the apoptotic response to chemotherapy and clinical outcome in breast cancer. Cancer Cell *21*, 793–806.

Jiang, Z., Deng, T., Jones, R., Li, H., Herschkowitz, J.I., Liu, J.C., Weigman, V.J., Tsao, M.S., Lane, T.F., Perou, C.M., and Zacksenhaus, E. (2010). Rb deletion in mouse mammary progenitors induces luminal-B or basal-like/EMT tumor subtypes depending on p53 status. J. Clin. Invest. *120*, 3296–3309.

Jonkers, J., Meuwissen, R., van der Gulden, H., Peterse, H., van der Valk, M., and Berns, A. (2001). Synergistic tumor suppressor activity of BRCA2 and p53 in a conditional mouse model for breast cancer. Nat. Genet. *29*, 418–425.

Kamura, T., Hara, T., Matsumoto, M., Ishida, N., Okumura, F., Hatakeyama, S., Yoshida, M., Nakayama, K., and Nakayama, K.I. (2004). Cytoplasmic ubiquitin ligase KPC regulates proteolysis of p27(Kip1) at G1 phase. Nat. Cell Biol. *6*, 1229–1235.

Kang, T.W., Yevsa, T., Woller, N., Hoenicke, L., Wuestefeld, T., Dauch, D., Hohmeyer, A., Gereke, M., Rudalska, R., Potapova, A., et al. (2011). Senescence surveillance of pre-malignant hepatocytes limits liver cancer development. Nature *479*, 547–551.

Kiyokawa, H., Kineman, R.D., Manova-Todorova, K.O., Soares, V.C., Hoffman, E.S., Ono, M., Khanam, D., Hayday, A.C., Frohman, L.A., and Koff, A. (1996). Enhanced growth of mice lacking the cyclin-dependent kinase inhibitor function of p27(Kip1). Cell *85*, 721–732.

Krtolica, A., Parrinello, S., Lockett, S., Desprez, P.Y., and Campisi, J. (2001). Senescent fibroblasts promote epithelial cell growth and tumorigenesis: a link between cancer and aging. Proc. Natl. Acad. Sci. USA *98*, 12072–12077.

Kuilman, T., and Peeper, D.S. (2009). Senescence-messaging secretome: SMS-ing cellular stress. Nat. Rev. Cancer *9*, 81–94.

Leng, R.P., Lin, Y., Ma, W., Wu, H., Lemmers, B., Chung, S., Parant, J.M., Lozano, G., Hakem, R., and Benchimol, S. (2003). Pirh2, a p53-induced ubiquitin-protein ligase, promotes p53 degradation. Cell *112*, 779–791.

Lin, H.K., Chen, Z., Wang, G., Nardella, C., Lee, S.W., Chan, C.H., Yang, W.L., Wang, J., Egia, A., Nakayama, K.I., et al. (2010). Skp2 targeting suppresses tumorigenesis by Arf-p53-independent cellular senescence. Nature *464*, 374–379.

Marino, S., Vooijs, M., van Der Gulden, H., Jonkers, J., and Berns, A. (2000). Induction of medulloblastomas in p53-null mutant mice by somatic inactivation of Rb in the external granular layer cells of the cerebellum. Genes Dev. *14*, 994–1004.

McClendon, A.K., Dean, J.L., Ertel, A., Fu, Z., Rivadeneira, D.B., Reed, C.A., Bourgo, R.J., Witkiewicz, A., Addya, S., Mayhew, C.N., et al. (2011). RB and p53 cooperate to prevent liver tumorigenesis in response to tissue damage. Gastroenterology *141*, 1439–1450.

Meuwissen, R., Linn, S.C., Linnoila, R.I., Zevenhoven, J., Mooi, W.J., and Berns, A. (2003). Induction of small cell lung cancer by somatic inactivation of both Trp53 and Rb1 in a conditional mouse model. Cancer Cell *4*, 181–189.

Nakayama, K., Ishida, N., Shirane, M., Inomata, A., Inoue, T., Shishido, N., Horii, I., Loh, D.Y., and Nakayama, K.-i. (1996). Mice lacking p27(Kip1) display increased body size, multiple organ hyperplasia, retinal dysplasia, and pituitary tumors. Cell *85*, 707–720.

Nakayama, K., Nagahama, H., Minamishima, Y.A., Matsumoto, M., Nakamichi, I., Kitagawa, K., Shirane, M., Tsunematsu, R., Tsukiyama, T.I., Ishida, N., et al. (2000). Targeted disruption of Skp2 results in accumulation of cyclin E and p27(Kip1), polyploidy and centrosome overduplication. EMBO J. *19*, 2069–2081.

Nakayama, K., Nagahama, H., Minamishima, Y.A., Miyake, S., Ishida, N., Hatakeyama, S., Kitagawa, M., Iemura, S., Natsume, T., and Nakayama, K.I. (2004). Skp2-mediated degradation of p27 regulates progression into mitosis. Dev. Cell *6*, 661–672.

Nickeleit, I., Zender, S., Sasse, F., Geffers, R., Brandes, G., Sörensen, I., Steinmetz, H., Kubicka, S., Carlomagno, T., Menche, D., et al. (2008). Argyrin a reveals a critical role for the tumor suppressor protein p27(kip1) in mediating antitumor activities in response to proteasome inhibition. Cancer Cell *14*, 23–35.

Old, J.B., Kratzat, S., Hoellein, A., Graf, S., Nilsson, J.A., Nilsson, L., Nakayama, K.I., Peschel, C., Cleveland, J.L., and Keller, U.B. (2010). Skp2 directs Myc-mediated suppression of p27Kip1 yet has modest effects on Myc-driven lymphomagenesis. Mol. Cancer Res. *8*, 353–362.

Park, J.H., Walls, J.E., Galvez, J.J., Kim, M., Abate-Shen, C., Shen, M.M., and Cardiff, R.D. (2002). Prostatic intraepithelial neoplasia in genetically engineered mice. Am. J. Pathol. *161*, 727–735.

Sage, J., Miller, A.L., Pérez-Mancera, P.A., Wysocki, J.M., and Jacks, T. (2003). Acute mutation of retinoblastoma gene function is sufficient for cell cycle re-entry. Nature *424*, 223–228.

Sherr, C.J. (2012). Ink4-Arf locus in cancer and aging. Wiley interdisciplinary reviews. Dev. Biol. *1*, 731–741.

Soucy, T.A., Smith, P.G., Milhollen, M.A., Berger, A.J., Gavin, J.M., Adhikari, S., Brownell, J.E., Burke, K.E., Cardin, D.P., Critchley, S., et al. (2009). An inhibitor of NEDD8-activating enzyme as a new approach to treat cancer. Nature *458*, 732–736.

Sun, D., Melegari, M., Sridhar, S., Rogler, C.E., and Zhu, L. (2006). Multi-miRNA hairpin method that improves gene knockdown efficiency and provides linked multi-gene knockdown. Biotechniques *41*, 59–63.

Walkley, C.R., Qudsi, R., Sankaran, V.G., Perry, J.A., Gostissa, M., Roth, S.I., Rodda, S.J., Snay, E., Dunning, P., Fahey, F.H., et al. (2008). Conditional mouse osteosarcoma, dependent on p53 loss and potentiated by loss of Rb, mimics the human disease. Genes Dev. *22*, 1662–1676.

Wang, H., Bauzon, F., Ji, P., Xu, X., Sun, D., Locker, J., Sellers, R.S., Nakayama, K., Nakayama, K.I., Cobrinik, D., and Zhu, L. (2010). Skp2 is required for survival of aberrantly proliferating Rb1-deficient cells and for tumorigenesis in Rb1+/- mice. Nat. Genet. *42*, 83–88.

Wei, C.L., Wu, Q., Vega, V.B., Chiu, K.P., Ng, P., Zhang, T., Shahab, A., Yong, H.C., Fu, Y., Weng, Z., et al. (2006). A global map of p53 transcription-factor binding sites in the human genome. Cell *124*, 207–219.

Wu, X., Wu, J., Huang, J., Powell, W.C., Zhang, J., Matusik, R.J., Sangiorgi, F.O., Maxson, R.E., Sucov, H.M., and Roy-Burman, P. (2001). Generation of a prostate epithelial cell-specific Cre transgenic mouse model for tissue-specific gene ablation. Mech. Dev. *101*, 61–69.

Wu, L., Grigoryan, A.V., Li, Y., Hao, B., Pagano, M., and Cardozo, T.J. (2012). Specific small molecule inhibitors of Skp2-mediated p27 degradation. Chem. Biol. *19*, 1515–1524.

Xuan, Z., Zhao, F., Wang, J., Chen, G., and Zhang, M.Q. (2005). Genome-wide promoter extraction and analysis in human, mouse, and rat. Genome Biol. *6*, R72.

Zhou, Z., Flesken-Nikitin, A., Corney, D.C., Wang, W., Goodrich, D.W., Roy-Burman, P., and Nikitin, A.Y. (2006). Synergy of p53 and Rb deficiency in a conditional mouse model for metastatic prostate cancer. Cancer Res. *66*, 7889–7898.

Zhu, W., Chen, Y., and Dutta, A. (2004). Rereplication by depletion of geminin is seen regardless of p53 status and activates a G2/M checkpoint. Mol. Cell. Biol. *24*, 7140–7150.

Cancer Cell, Volume *24*

Supplemental Information

Skp2 Deletion Unmasks a p27 Safeguard that Blocks Tumorigenesis in the Absence of pRb and p53 Tumor Suppressors

Hongling Zhao, Frederick Bauzon, Hao Fu, Zhonglei Lu, Jinhua Cui, Keiko Nakayama, Keiich I. Nakayama, Joseph Locker, and Liang Zhu

Supplemental Data

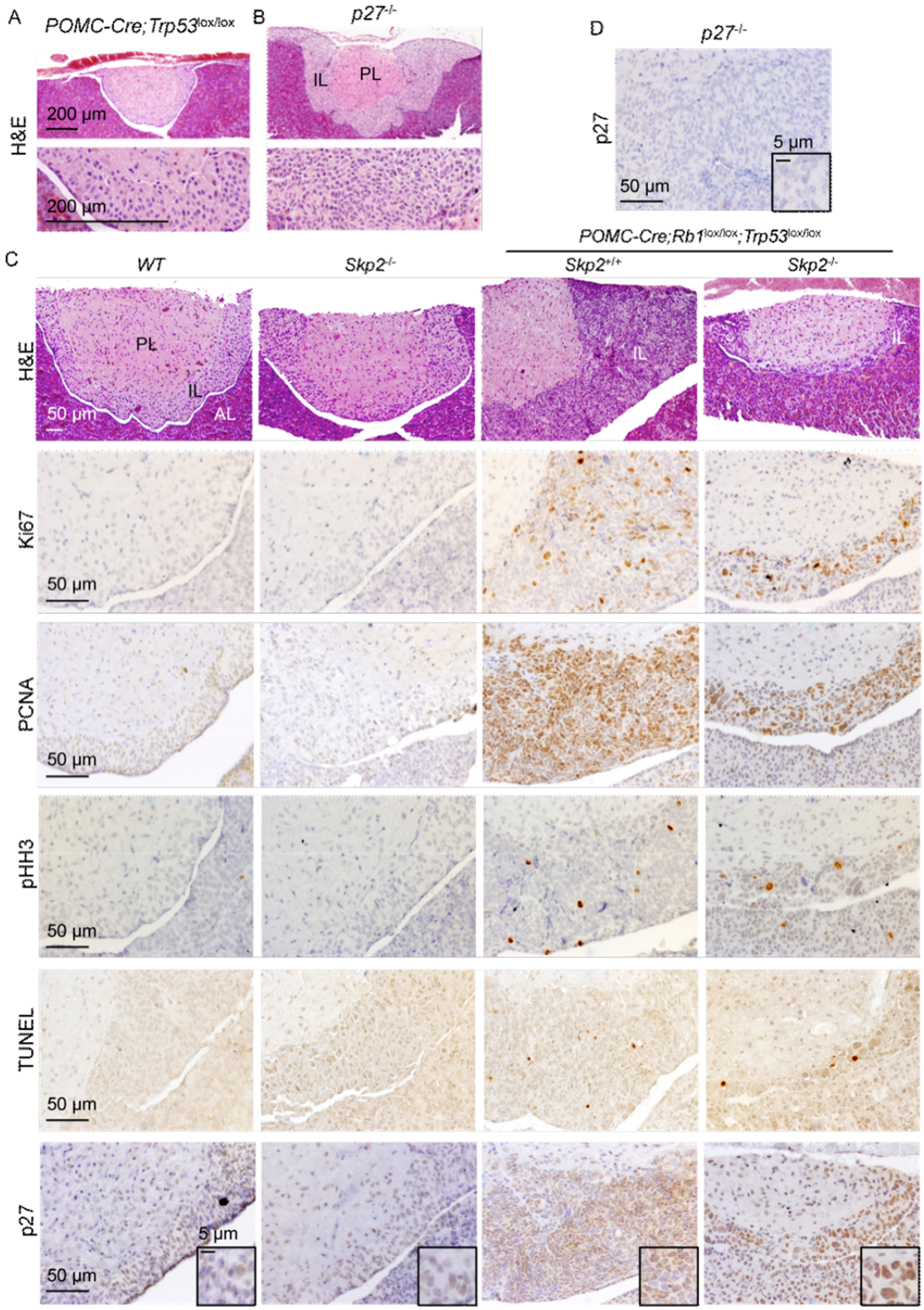

Figure S1. Related to Figure 1. (A and B) H&E staining of pituitary sections of 7 weeks old *POMC-Cre;Trp53*$^{lox/lox}$ (A) or *p27*$^{-/-}$ (B) mice. (C) Pituitary sections of the indicated genotypes were stained as indicated. (D) Pituitary sections of *p27*$^{-/-}$ mice stained with anti-p27.

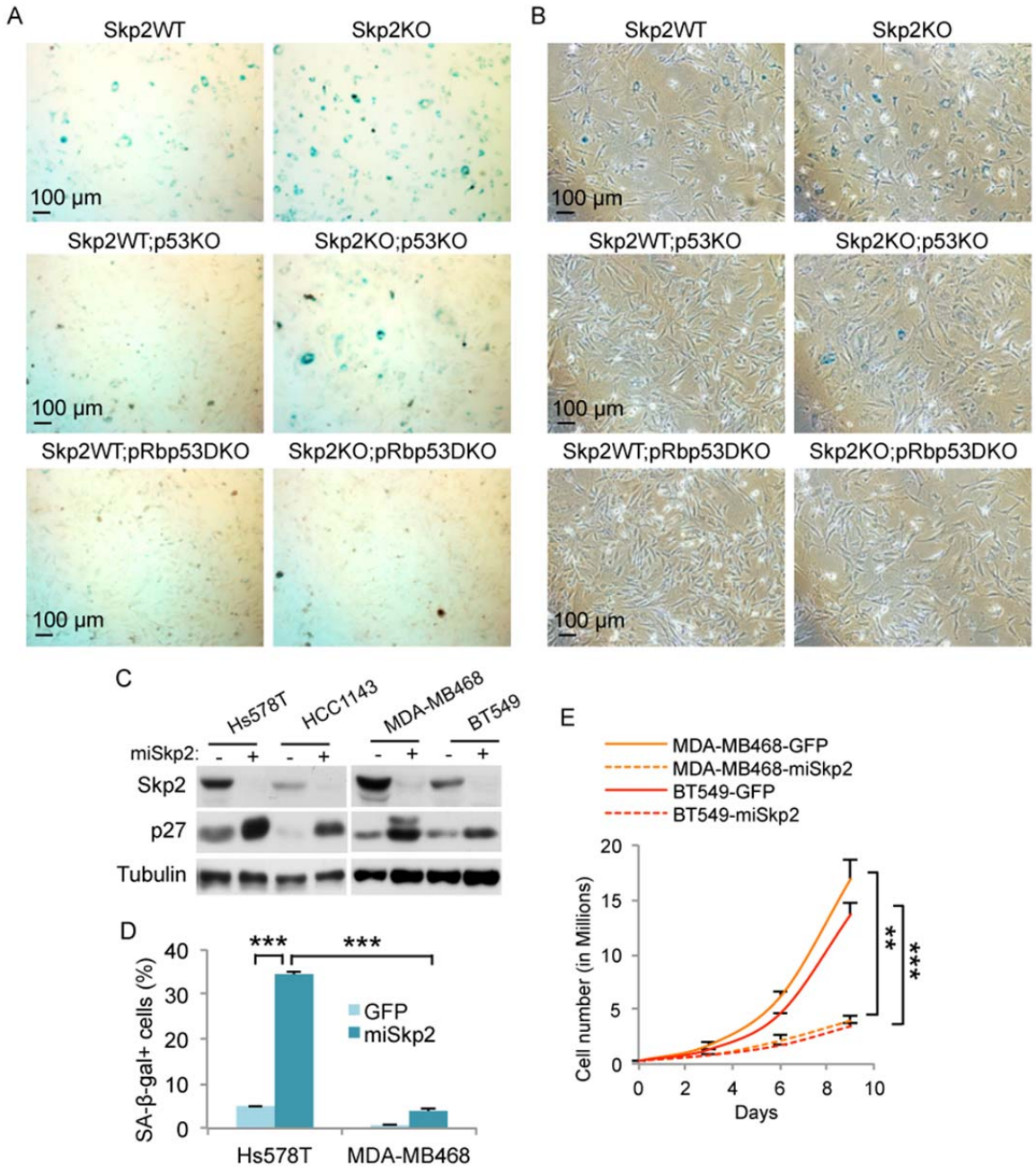

Figure S2. Related to Figure 2. (A and B) MEFs of the indicated genotypes were stained with SA-β-gal and photographed in bright field (A) or in phase contrast (B). (C) Indicated human breast cancer cell lines, with or without Skp2 knockdown (miSkp2) were subjected to Western blot. (D) Quantification of SA-β-gal stain in photographs shown in Figure 2B. (E) Actual cell proliferations for the indicated human breast cancer cells expressing GFP or miSkp2. Quantitative data are presented as average +/- SEM. Student's *t* test was used for statistical analysis. **, $p < 0.01$; ***, $p < 0.002$.

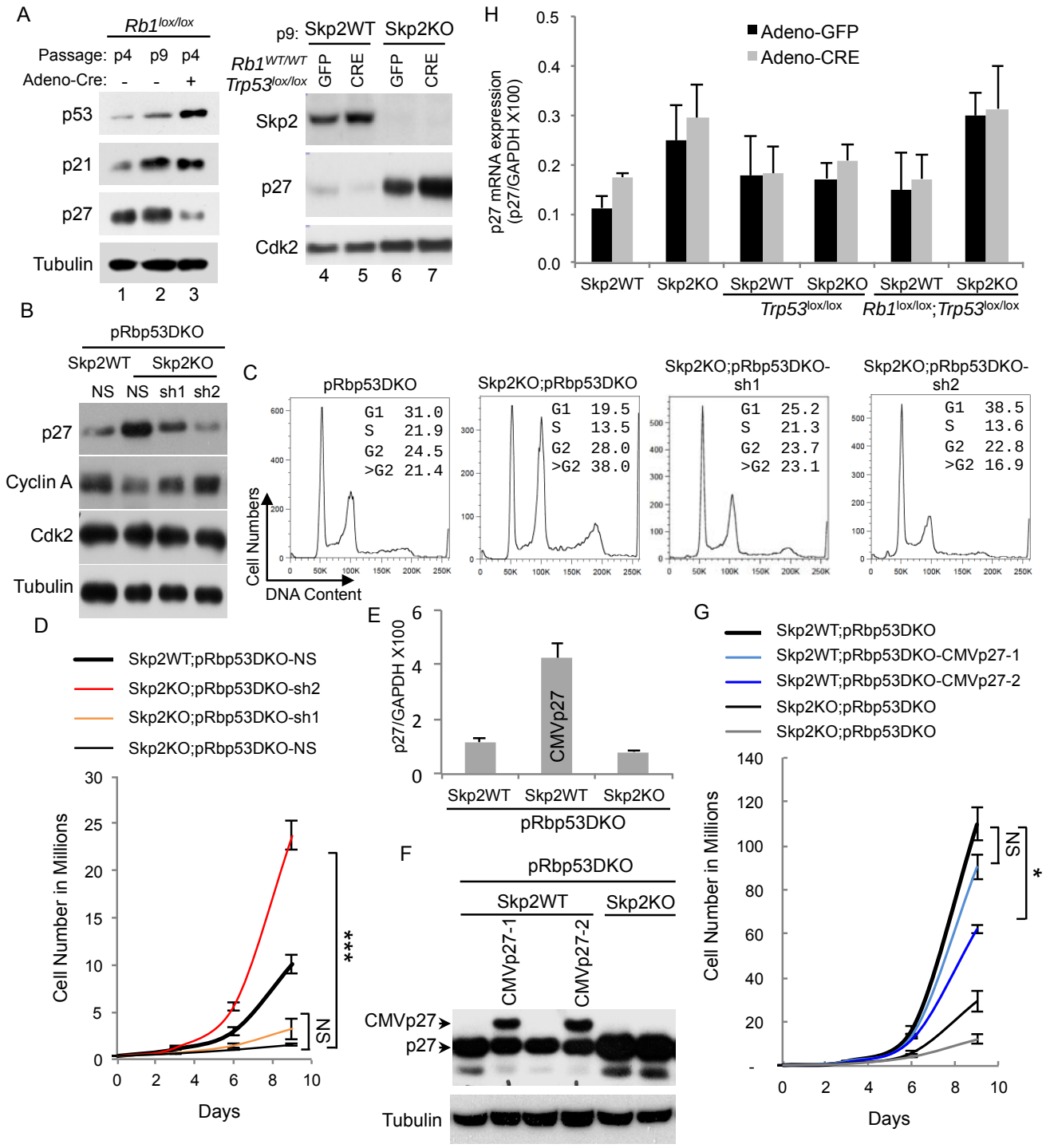

Figure S3. Related to Figure 3. (A) Western blots of indicated MEFs. MEF cultures established from dissected embryos on previous days are "Passage" 1 (p1). (B) Western blots of indicated MEFs transduced with indicated knockdown hairpins. NS, non-specific random sequence hairpins. (C) DNA content FACS. (D) Same cells as in (C) were counted to determine actual cell proliferation. (E) RT-qPCR of p27 mRNA from indicated MEFs. (F) Western blot of cell in (E). (G) Proliferation curves of the indicated cells. (H) RT-qPCR of p27 mRNA. Quantitative data are presented as average +/- SEM. Student's *t* test was used for statistical analysis. *, $p < 0.05$; ***, $p < 0.002$; NS, $p > 0.05$.

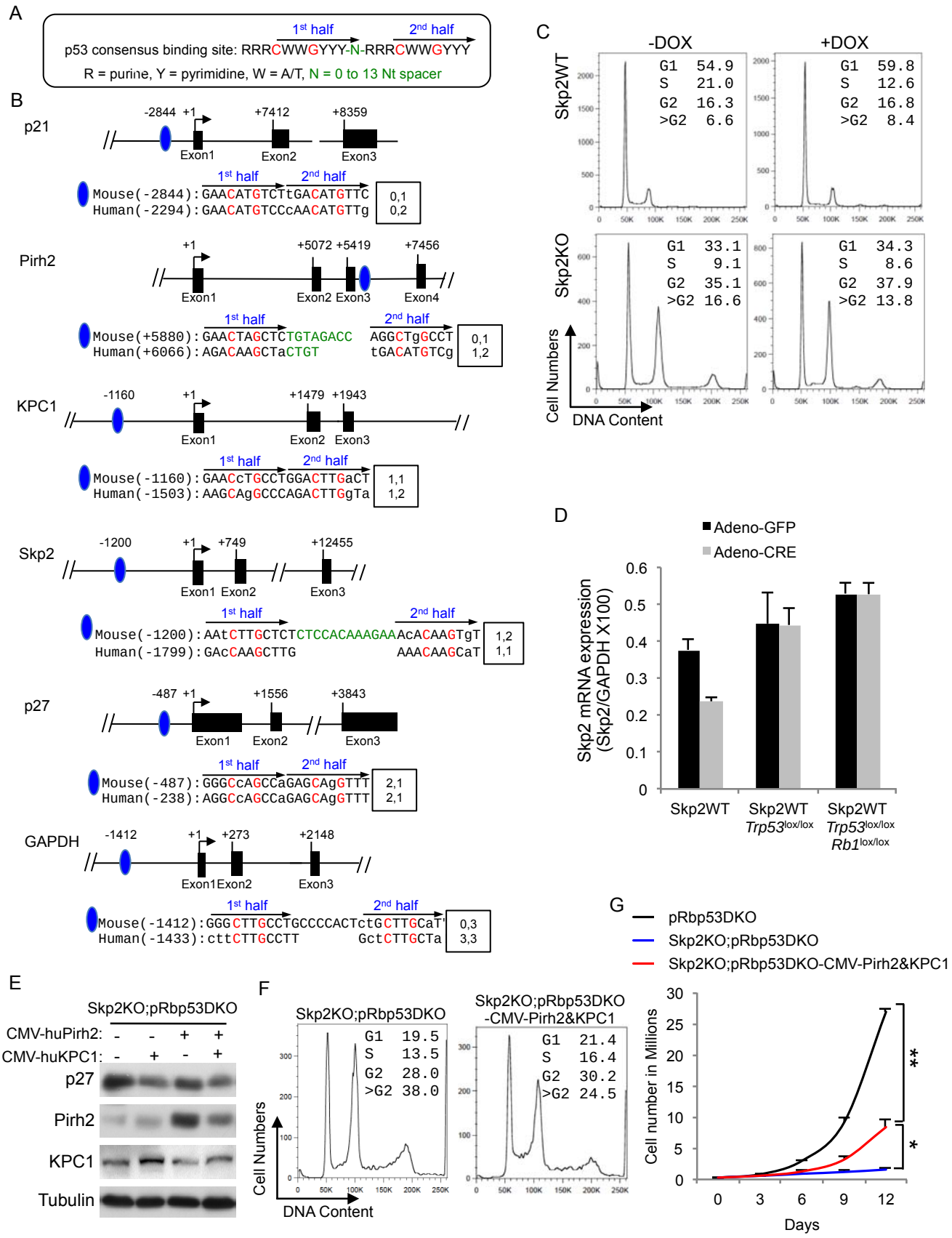

<< Continued on the next page >>

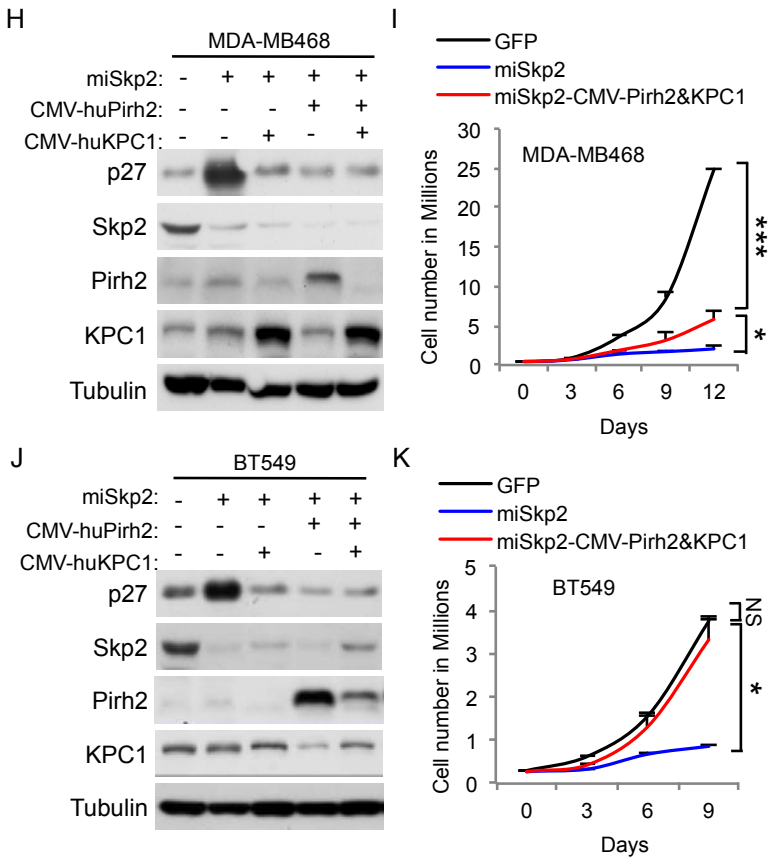

Figure S4. Related to Figure 4. (A) The consensus p53 binding site. (B) The best matching sequence to the consensus p53 binding site for each genes. Conservations between mouse and human are indicated. (C) DNA content FACS showing cell cycle profiles of WT and Skp2KO MEFs before and after DOX treatment, as in Figure 4A to 4C. (D) Effects of deleting *Trp53* alone or together with *Rb1* on mRNA levels of Skp2 is measured by RT-qPCR. (E to G) Expression of human Pirh2 and KPC1 from a CMV promoter was examined by western blots (E), their effects on cell cycle profiles were determined by DNA content FACS (F), and their effects on actual cell proliferation by cell number counts for 12 days (G). (H to K) Expression of CMV-huPirh2 and CMV-huKPC1 in human breast cancer cell lines were examined by Western blots (H and J) and their effects on cell proliferation by cell number counts (I and K). Quantitative data are presented as average +/- SEM. Student's *t* test was used for statistical analysis. *, $p < 0.05$; **, $p < 0.01$; ***, $p < 0.002$; NS, $p > 0.05$.

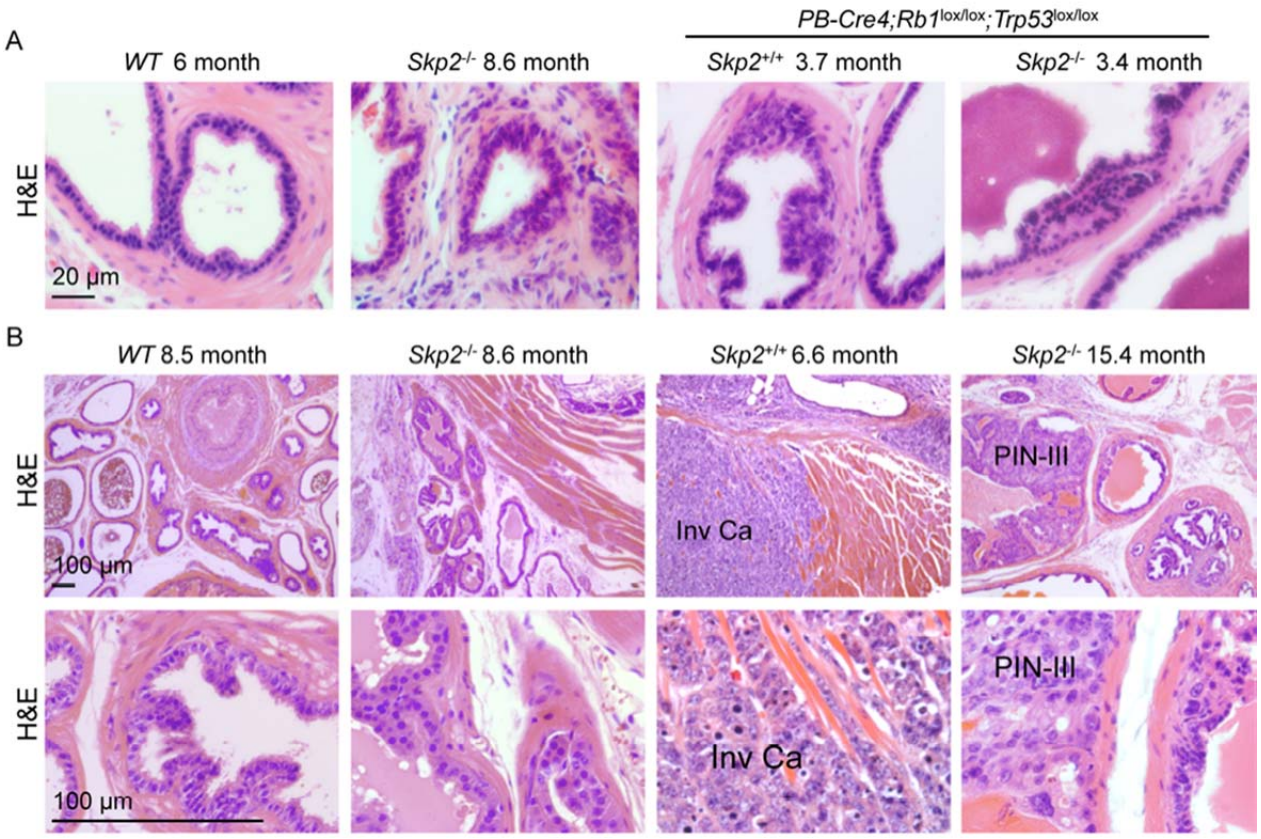

Figure S5. Related to Figure 5. (A) PINs at 3 months. (B) Invasive carcinoma in the presence of Skp2 at 6.6 month, and PIN-III in the absence of Skp2 at 15.4 month. Two magnifications are shown.

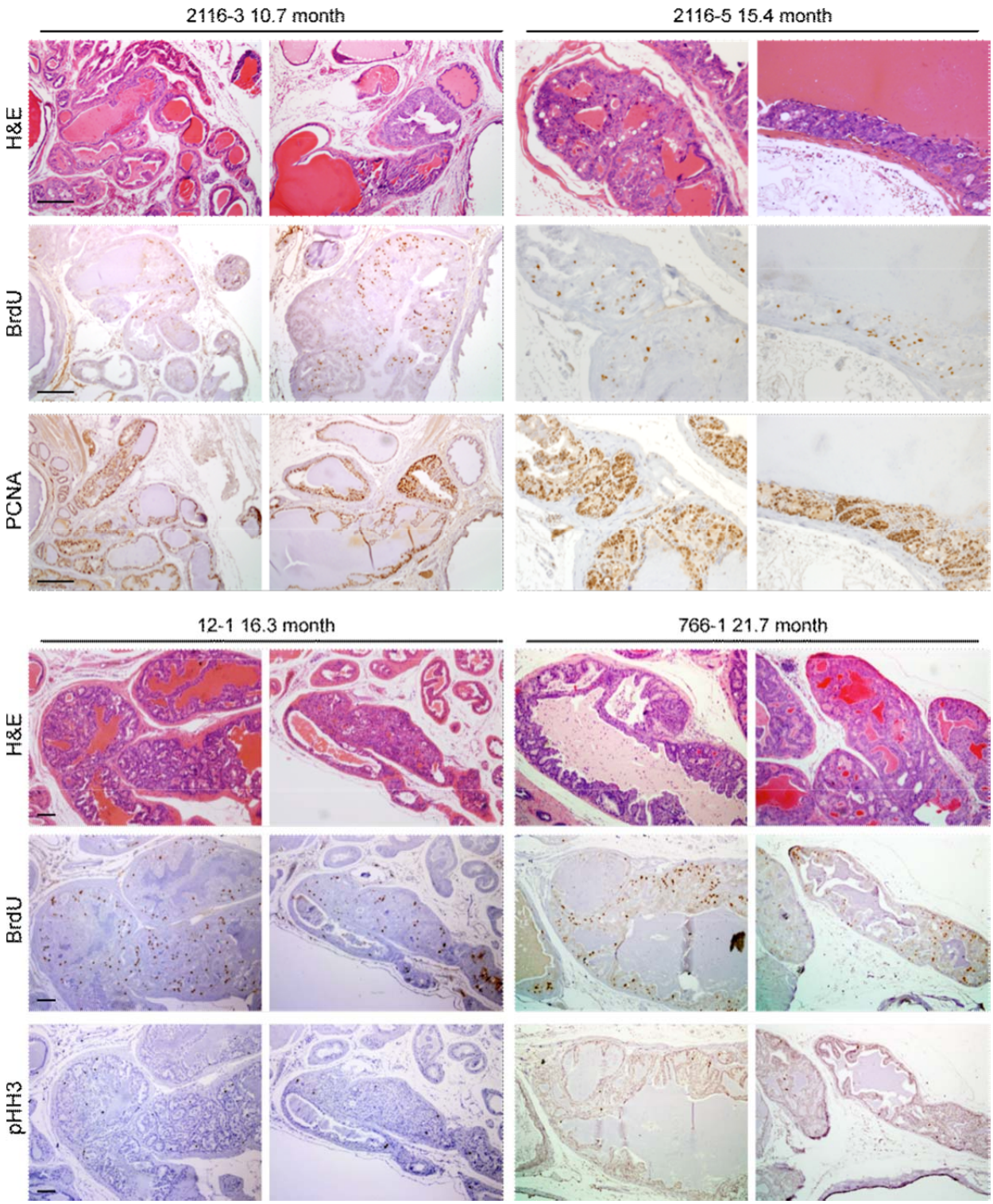

Figure S6. Related to Figure 7. Prostate sections from *Skp2*$^{-/-}$*;PB-Cre4;Rb1*$^{lox/lox}$*;Trp53*$^{lox/lox}$ mice in the 10-22 months age group (with their IDs) were analyzed with H&E, BrdU (2 hr labeling), PCNA, and pHH3 staining, as indicated. Scale bars = 100 μm.

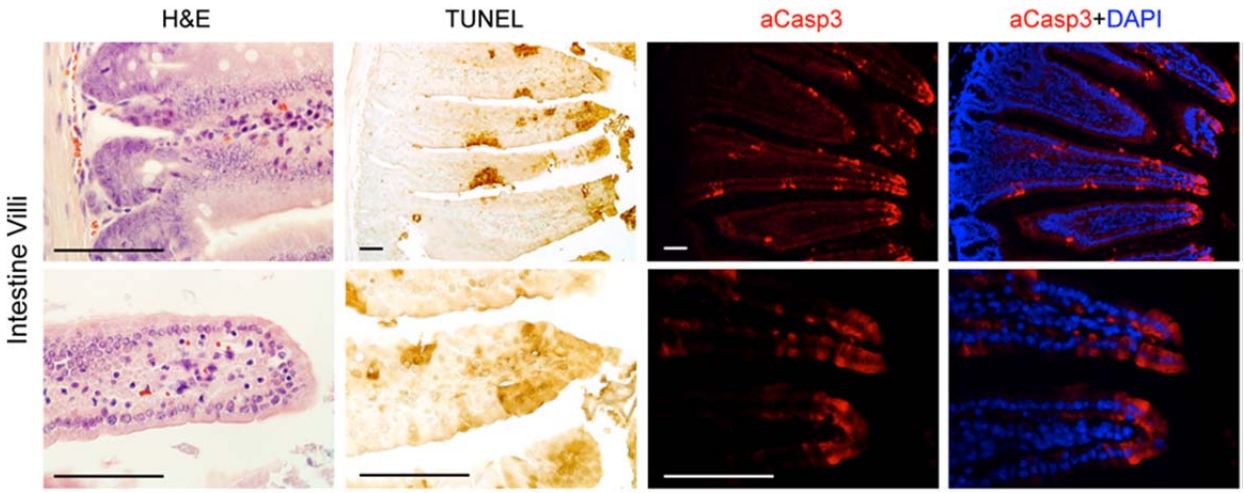

Figure S7. Related to Figure 8. Validation of TUNEL and aCasp3 staining for apoptosis with the characteristic distribution of apoptotic cells in intestine villi. Scale bars = 50 μm.

Supplemental Experimental Procedures

Mouse genotyping. For *POMC-Cre* transgenic mice: POMC-Cre-F: 5'-TGGCTCAATGTCCTTCCTGG-3' and POMC-Cre-R: 5'-GAAATCAGTGCGTTCGAACGCTAGA-3'. The transgene yields a PCR product of 400bp. For $Rb1^{lox/lox}$ mice: Rblox-F: 5'-CTCTAGATCCTCTCATTCTTC-3' and Rblox-R: 5'-CCTTGACCATAGCCCAGCAC-3'. The Rblox allele yields a PCR product of 310bp while the wild type allele a 250bp PCR product. For $Trp53^{lox/lox}$ mice: p53lox-F: 5'-CACAAAAACAGGTTAAACCCAG-3' and p53lox-R: 5'-AGCACATAGGAGGCAGAGAC-3'. The p53lox allele yields a PCR product of 370bp while the wild type allele a 288bp PCR product. For $Skp2^{+/-}$ mice: wild type allele, KN3: 5'-AGAGTGGAAGAACCCAGGCAGGAC-3' and KN4: 5'-CCCGTGGAGGGAAAAAGAGGGACG-3', yielding a 430bp PCR product, and KO allele: KN13: 5'- GCATCGCCTTCTATCGCCTTCTTG-3' and KN38: 5'-TTCCCACCCCCACATCCAGTCATT-3' yielding a PCR product of 500bp. For *PB-Cre4* mice: PB-CRE4-F: 5'-CTGAAGAATGGGACAGGCATTG-3' and PB-CRE4-R: 5'-CATCACTCGTTGCATCGACC-3'. The PB-Cre4 transgene yields a PCR product of 393bp. For $p27^{+/-}$ mice: WT-F: 5'-GATGGACGCCAGACAAGC-3' and WT-R: 5'-AGGGGCTTATGATTCTGAAAGTCG-3', p27KO-F: 5'-CCTTCTATCGCCTTCTTG-3' and p27KO-R: 5'-TGGAACCCTGTGCCATCTCTAT-3'. WT allele yields a PCR product of 166bp, KO allele a 500bp PCR product.

MEF preparation and infection. Embryos from timed pregnancies were harvested between E12.5-E14.5. Heads, livers, and blood clots were removed and the rest of tissues were minced and put into 1 ml Trypsin (25300-054, Gibco) for 10 min at 37°C. The tissue and Trypsin mixture was pipetted up and down several times and the dissociated cells were cultured in DMEM (11965-092, Giboco) containing 10% FBS (S11550, Atlanta Biologicals) and 1% Pen/Strep (15140-122, Giboco). Cells were split every 3-4 days during early passages, and MEFs at passage 2 or 3 were used for infection to delete, knockdown or overexpress specific proteins. Adeno-GFP and Adeno-CRE viruses were from Einstein Gene therapy Core, lentivirus vectors expressing p27, p53, or shRNAs from Einstein shRNA Core facility. Lentiviral helper constructs were from L. Naldini and A. Follenzi (Follenzi et al., 2000) and Xia Wang of Einstein Gene therapy Core. Lentivirus stocks were generated and concentrated as described previously (Sun et al., 2006).

SA-β-gal stain. To determine cellular senescence, MEFs and human breast cancer cell lines were plated in triplicate 6 cm plates for 3 days, and were fixed with 0.2% glutaraldehyde (G5882, Sigma-Aldrich) for 15 minutes at room temperature. SA-β-gal activity was determined by staining cells with SA-β-gal staining solution (5 mM Potassium Ferrocyanide, 5 mM Potassium Ferricyanide, 2 mM $MgCl_2$, 150

mM NaCl, 40 mM citric acid/sodium phosphate buffer pH6.0, and 1 mg/ml X-gal) for 16 hr (MEFs) and 5 hr (human cancer cell lines) at 37°C. Results were quantified under microscope.

FACS. Cells were washed and fixed by adding 6 ml ice-cold 80% EtOH (~70% EtOH final) while vortexing. Cells were then washed with 5 ml PBS and resuspended in 0.5 ml of 0.25 mg/ml RNase A and 10 µg/ml propidium iodide in PBS for FACS analysis. BrdU labeling was for 30 min in 10 µM BrdU. After EtOH fixation for 30 minutes in 4˚C, cells were incubated in 1 ml 2 M HCl, 0.5% Triton X-100 for 30 min at room temperature, neutralized in 1 ml 0.1 M Sodium Borate pH9.0, and resuspended in 100-200 µl 0.2% BSA/0.5% Tween 20/PBS for 5 min. We used 20 µl anti-BrdU-FITC per 10^6 cells and incubated for 30-60 min at room temperature. Staining for pHH3 was performed with the same steps as anti-BrdU. FACS and data analysis were performed together with the Einstein FACS Core.

Cell proliferation assay. $3X10^5$ cells were plated in 6 cm plates in triplicate, and cell numbers were counted every 2 or 3 days under the microscope with hemocytometers for indicated days.

Western blot. MEF lysates were prepared with RIPA buffer (50 mM Tris-HCl pH7.4, 1% NP40, 0.5% sodium deoxycholate, 0.1% SDS, 1 mM EDTA, 150 mM NaCl, and standard protease inhibitors). Prostate tissues or tumors were snap-frozen in dry ice and stored in −80 °C. Frozen tissues were homogenized with Dounce glass homogenizer in tissue lysis buffer (50 mM HEPES, pH 7.2, 150 mM NaCl, 1 mM EDTA, 0.1% Tween-20, 1 mM dithiothreitol and standard protease inhibitors). Debris was removed by centrifugation for 10 min at 14,000 r.p.m. in an Eppendorf Centrifuge 5415C at 4 °C. Protein concentrations of the extracts were determined by Bio-Rad protein assay kit, and equal amounts of protein samples were loaded on 10% SDS gels and blotted onto polyvinylidene fluoride membrane.

RT-qPCR. RNA was extracted by Trizol reagent (Invitrogen). Oligo-dT and SuperScript II (Invitrogen) were used for the synthesis of the first-strand cDNA at 42 °C for 60 min. The qPCR primers for mouse Skp2, p21, p27, KPC1, Pirh2 and GAPDH are listed below. SYBR Green PCR Master Mix (4309155, ABI) and the standard program of ABI 7500 Fast real-time PCR were used.

ChIP and qPCR. MEFs were cross-linked with 1% formaldehyde (#252549, Sigma-Aldrich) in culture medium for 10 min at room temperature. Cross-link was stopped by addition of glycine to a final concentration of 0.125 M for 5 min at room temperature. Fixed cells were scraped off the plates, washed twice with PBS, pelleted and stored. Cell pellets were re-suspended in 1 ml of cell lysis buffer containing PMSF (5 mM HEPES pH8.0, 85 mM KCl, 0.5% Triton X-100,) and put on ice for 20 min before being pelleted again by centrifugation at 2500g for 5 minutes. Pellets were re-suspended with 600 µl nuclear lysis buffer containing PMSF (50 mMTris-HCl pH8.0, 10 mM EDTA, 1% SDS). DNA was sheared by sonication for 15 s x 4 in a 60 Sonic Dismembrator (Fisher), at a power setting of 10. The resultant genomic DNA fragments with a bulk size of 100–1000 bp were precleared by addition of 20 µl of blocked protein A-Agrose beads (P9269, Sigma). The beads were blocked with tRNA and Salmon sperm DNA. The precleared chromatin were incubated overnight at 4°C with 2 µg antibody (for p53, SC-71817X, Santa Cruz Biotechnology). The chromatin and antibody mixture were then incubated with blocked protein A-Agrose beads at 4°C for 4 hr with rotation and followed by successive 10-minute washes in 1 ml of IP dilution buffer (16.7 mM Tris-HCl pH 8.0, 167 mM NaCl, 1.2 mM EDTA, 1% Triton X-100, and 0.01% SDS), dialysis buffer (2 mM EDTA, 50 mM Tris-HCl pH 8.0, 0.2% Sarkosyl), TSE-500 buffer (2 mM EDTA, 20 mM Tris-HCl pH 8.0, 500 mM NaCl, 1% Triton X-100, and 0.1% SDS), LiCl detergent buffer (100 mM Tris-HCl pH 8.0, 1% deoxycholic acid, 1% Triton X-100, 500 mM LiCl), and TE buffer. After washing, the samples were eluted with elution buffer (50 mM $NaHCO_3$, 1% SDS). The eluted material was purified by Qiagen PCR purification kit for qPCR.

Tissue preparation and staining. Tissues were fixed in 10% Formalin (SF 100-4, Fisher Scientific), embedded in paraffin wax and sectioned. Paraffin sections were processed according to protocols for the SuperPicture™ kit (879263 and 879163, Invitrogen). Secondary antibodies for IHC were HRP polymer conjugated anti-rabbit or anti-mouse IgG. Color development was by DAB chromogen supplied in the SuperPicture™ kit. Sections were counterstained by Harris Hematoxylin (S212, Poly Scientific). Immunofluorescence detection was by Rhodamine conjugated goat anti-rabbit-IgG (SC-2091, Santa Cruz Biotechnology) or Fluorescein conjugated horse-anti-mouse-IgG (FI-2000, Vector laboratory).

TSA™PLUS Fluorescence Kit (NEL741001KT, PerkinElmer) was used to amplify signals when indicated. DNA was stained with DAPI. Feulgen staining was done with Schiff's reagent (s272, Poly Scientific R&D Corp.), and counter stained with fast green (s2114, Poly Scientific R&D Corp.).

DNA content analysis with tissue sections. DAPI stained prostate sections were scanned and analyzed by the iCys® Research Imaging Cytometer and iCys® Cytometric Analysis Software (CompuCyte Corporation). At least 500 prostate epithelial cells were analyzed for each genotype.

Primer sequences

qPCR primers	
GAPDH	
GAPDH-F	5'-AATGTGTCCGTCGTGGATCT-3'
GAPDH-R	5'-GGTCCTCAGTGTAGCCCAAG-3'
p27	
p27-F	5'-GCGGTGCCTTTAATTGGGTCT-3'
p27-R	5'-GGCTTCTTGGGCGTCTGC T-3'
p21	
p21-F	5'-CCCGAGAACGGTGGAACTT-3'
p21-R	5'-TGCAGCAGGGCAGAGGAA-3'
Skp2	
Skp2-F	5'-CCAGCAAGACTTCTGAACTGC-3'
Skp2-R	5'-GAGGCACAGACAGGAAAAGA-3'
KPC1	
KPC1-F	5'-GAAGTCCAGGGTCACAGGCA-3'
KPC1-R	5'-GGTTATGGAAGTTTAGCGGTT T-3'
Pirh2	
Pirh2-F	5'-GCCTTAGACATGACTCGGTAC-3'
Pirh2-R	5'-CTGCTGATCCACTGGCACTCT-3'
ChIP primers	
GAPDH	
GAPDH-F	5'-GAGTTCTGGGAGTCTCGTGG-3'
GAPDH-R	5'-CTCTTCGGGTGGTGGTTCA-3'
p21	
p21-F	5'- TTCAGTGCAGGGTGGTGGA-3'
p21-R	5'- ATTCTGCTGGCAAAGTGG G-3'
Pirh2	
Pirh2-F	5'- CATTTCTTCCCTCCGAACCCT-3'
Pirh2-R	5'- CTAGTTCCAGGACAGCCAAAG C-3'
KPC1	
KPC1-F	5'-GTAGGCAGGACTTAGGAGGGT-3'
KPC1-R	5'-GGATAGATGGTGGCAGGAAG-3'
Skp2	
Skp2-F	5'-TCTCCCCTGTTGCACAGTTT-3'
Skp2-R	5'-TGATGAGTCTCCCAAATACCA-3'
p27	
p27-F	5'-ACCGCCATATTGGGCAACTAAA-3'
p27-R	5'-GTGGCAAACAGTCGGAGCGTA-3'

Knockdown and overexpression vectors

Constructs	Packaging plasmids	Mammalian selection	Sequences
pGIP2-shp27-1	pCMV-dR8.91; pMD2-VSVG	Puromycin (10ug/ml)	5'-AGAAGATTCTTCTTCGCAA-3'
pGIP2-shp27-2	pCMV-dR8.91; pMD2-VSVG	Puromycin (10ug/ml)	5'-ACAATAACACTAAAATTTT-3'
Lenti-CMV-miSkp2	pMDLg/pRRE, pRSV-REV, and pMD2-VSVG	N/A	5′-CCTTAGACCTCACAGGTAA-3′
pLOC-p27	pCMV-dR8.91; pMD2-VSVG	Blasticidin (10ug/ml)	Human p27 ORF
pLX304-p53	pMDLg/pRRE,	Blasticidin	Human p53 ORF

	pRSV-REV, and pMD2-VSVG	(10ug/ml)	
pLOC-RNF123	pCMV-dR8.91; pMD2-VSVG	Blasticidin (10ug/ml)	Human KPC1 ORF
pLOC-RCHY1	pCMV-dR8.91; pMD2-VSVG	Blasticidin (10ug/ml)	Human Pirh2 ORF

Supplemental Reference

Follenzi, A., Ailles, L.E., Bakovic, S., Geuna, M., and Naldini, L. (2000). Gene transfer by lentiviral vectors is limited by nuclear translocation and rescued by HIV-1 pol sequences. Nat Genet *25*, 217-222.

Reply Reply All Forward

Cell Symposia: Hallmarks of Cancer: Poster Acceptance Letter

Content-CHAL2014 [Content-CHAL2014@elsevier...

To: Hongling Zhao

Monday, August 18, 2014 7:58 AM

Poster Acceptance Letter

Abstract reference number: CHAL2014_0167

Date: 18th August 2014

Email: hongling.zhao@einstein.yu.edu

Dear H. Zhao ,

Thank you for submitting an abstract to present at **Cell Symposia: Hallmarks of Cancer**. On behalf of the Organising Committee I am delighted to inform you that your abstract entitled "**Identifying effective antitumor mechanisms when both pRb and p53 are genetically inactivated**" has been accepted for **poster presentation** at the Conference.

If you have requested an oral slot, the review committee will finalise the decision on your abstract for short talk presentation in the next two weeks. We will contact you again by 29th August to confirm if your paper has been accepted for a short talk presentation

Title:	**Identifying effective antitumor mechanisms when both pRb and p53 are genetically inactivated**
Authors:	**H. Zhao, Z. Lu, L. Zhu**
Presenting Author:	**H. Zhao**

Please check the above details of your presentation carefully, as all conference material will be printed with this information. If there are any corrections please inform us as soon as possible by email to: Content-CHAL2014@elsevier.com

It is a condition of abstract acceptance that you or a nominated presenting co-author registers for the

Abstract for Cell Symposium, Hallmarks of Cancer: Asia, November 9-11, 2-14-Beijing, China

Identifying effective antitumor mechanisms when both pRb and p53 are genetically inactivated

Genetic inactivation of both major tumor suppressors pRb and p53 irreparably disables most cells' antitumor mechanisms. TCGA documents recurrent genetic inactivation of RB1 and TP53. They often co-occur and the co-occurrences become more frequent in more advanced cancer, which likely explain why advanced cancer are more likely to resist current anticancer therapies. Skp2 mediates ubiquitination of p27 to activate cyclin/CDKs, of Akt1 to promote anaerobic glycolysis, and of E-cadherin to promote cell migration. We used pRb and p53 doubly deficient mouse tumor models to determine the antitumor effects of targeting Skp2. Results show that Skp2 deletion blocked pRb and p53 doubly deficient pituitary and prostate tumorigenesis. On this platform, we identify multiple antitumor mechanisms, including mitotic block by p27, apoptosis by p73, blocking anaerobic glycolysis by targeting LDH-A, and dynamic control of EMT. We suggest that these antitumor mechanisms be considered in designing therapies for advanced and multi-therapy resistant cancer.

Reply Reply All Forward

Congratulations!

Mary Anne Clifford

To: Hongling Zhao

Cc: Liang Zhu

Tuesday, October 21, 2014 1:33 PM

You forwarded this message on 10/21/2014 1:47 PM.

October 21, 2014

Hongling Zhao, M.D., Ph.D.
Department of DMB
Ullmann - 521

Dear Hongling:

I am delighted to inform you that you have been selected by the Einstein Awards Committee as a recipient of one of the Dennis Shields Postdoctoral Research Prizes. Competition for these prizes was intense, and you should be extremely proud of this achievement.

Dean Spiegel will be presenting each awardee with a prize of $5,000 at a ceremony to be held at a date and time soon to be announced. In the spirit of the occasion, each awardee will be afforded the opportunity to give a 15-minute presentation of his/her work. Winners of travel awards for poster presentations will be announced at the close of the ceremony.

Please accept my congratulations on your truly outstanding achievement. I know that I speak for the entire Einstein community in wishing you continued success in your research, and I look forward to hearing your presentation.

With best wishes,

Jonathan M. Backer, M.D.
Director